



**HAL**  
open science

# Dynamic Cages-Towards Nanostructured Smart Materials

Wojciech Drożdż, Artur Ciesielski, Artur Stefankiewicz

► **To cite this version:**

Wojciech Drożdż, Artur Ciesielski, Artur Stefankiewicz. Dynamic Cages-Towards Nanostructured Smart Materials. *Angewandte Chemie International Edition*, 2023, 10.1002/anie.202307552 . hal-04238038

**HAL Id: hal-04238038**

**<https://hal.science/hal-04238038>**

Submitted on 13 Oct 2023

**HAL** is a multi-disciplinary open access archive for the deposit and dissemination of scientific research documents, whether they are published or not. The documents may come from teaching and research institutions in France or abroad, or from public or private research centers.

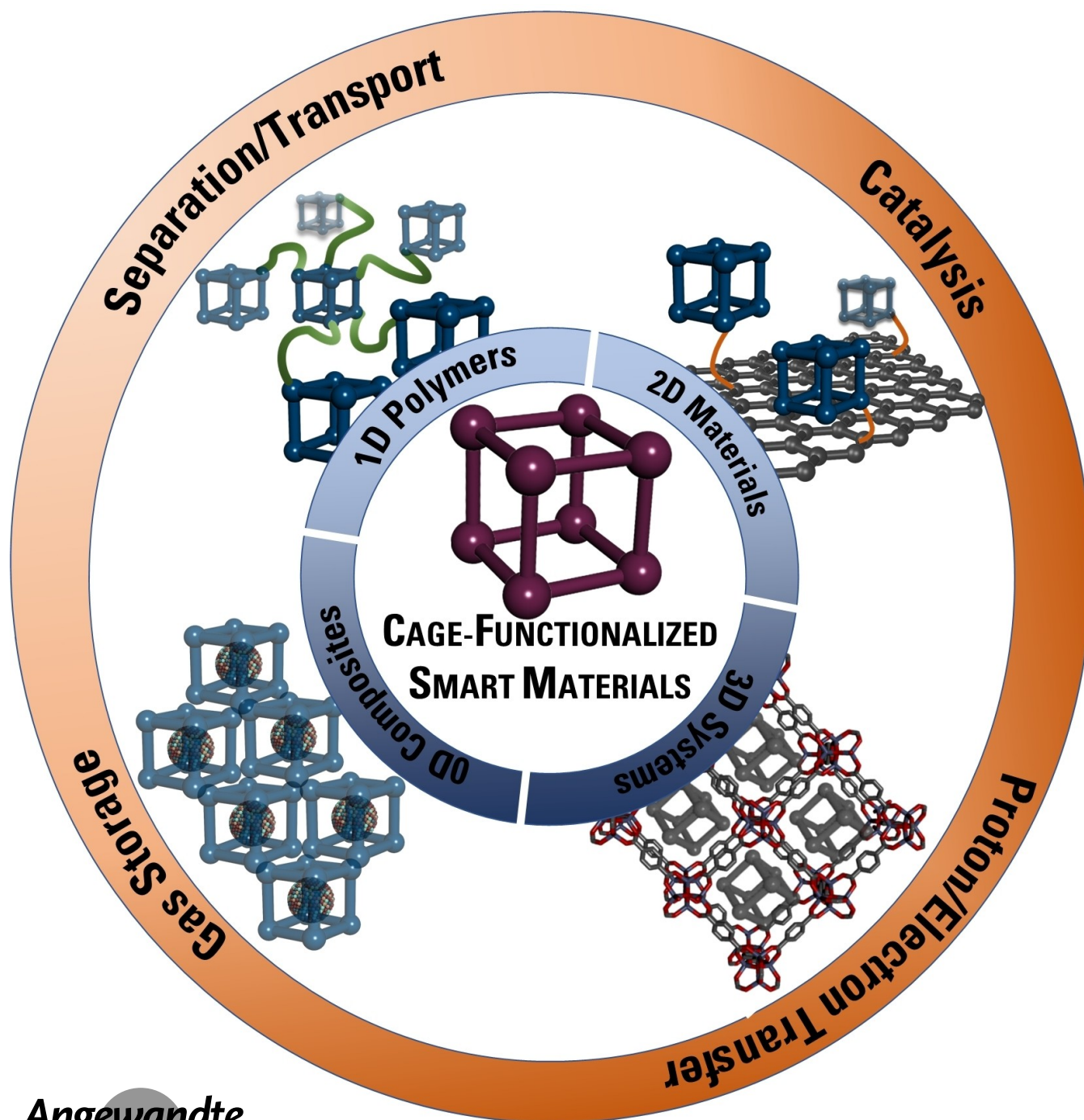
L'archive ouverte pluridisciplinaire **HAL**, est destinée au dépôt et à la diffusion de documents scientifiques de niveau recherche, publiés ou non, émanant des établissements d'enseignement et de recherche français ou étrangers, des laboratoires publics ou privés.

How to cite: *Angew. Chem. Int. Ed.* **2023**, e202307552  
doi.org/10.1002/anie.202307552

**Metal-Organic Cages****Dynamic Cages—Towards Nanostructured Smart Materials**

Wojciech Drożdż, Artur Ciesielski,\* and Artur R. Stefankiewicz\*

Dedicated to Professor Makoto Fujita on the occasion of his 65<sup>th</sup> birthday.



**Abstract:** The interest in capsular assemblies such as dynamic organic and coordination cages has blossomed over the last decade. Given their chemical and structural variability, these systems have found applications in diverse fields of research, including energy conversion and storage, catalysis, separation, molecular recognition, and live-cell imaging. In the exploration of the potential of these discrete architectures, they are increasingly being employed in the formation of more complex systems and smart materials. This Review highlights the most promising pathways to overcome common drawbacks of cage systems (stability, recovery) and discusses the most promising strategies for their hybridization with systems featuring various dimensionalities. Following the description of the most recent advances in the fabrication of zero to three-dimensional cage-based systems, this Review will provide the reader with the structure-dependent relationship between the employed cages and the properties of the materials.

## 1. Introduction

An ever-growing interest in porous compounds<sup>[1]</sup> with defined pore distributions and controllable pore sizes has resulted in the emergence of two classes of assemblies—extended frameworks and discrete hollow cages.<sup>[2]</sup> The most prominent example of extended, highly ordered porous compounds today is probably that of metal–organic frameworks (MOFs)—a class of crystalline materials with a periodic network structure resulting from the molecular self-assembly of metal ions or clusters and organic ligands—features that offer them far greater versatility than other three-dimensional porous species such as zeolites.<sup>[3,4]</sup> The design and synthesis of MOFs depend on reticular chemistry, which allows the preparation of specific structures through the selection of organic and inorganic components. The inorganic units determine the node connectivity while the organic linkers the number of nodes that will be interconnected. A similar approach can be employed to synthesize discrete coordination cages also referred to as metal-organic cages (MOCs).<sup>[5–8]</sup> Properly chosen organic ligands in combination with metal ions exhibiting defined coordination behavior (coordination number and predetermined geometries) allow the synthesis of various cage-type compounds with designed internal space, geometry, and functionality. Although MOCs share some similarities with MOFs, they are not infinite networks like MOFs. Rather, they are a class of discrete molecules with unique characteristics such as sizes, topologies, solubility, and chemical stability compared to MOFs.<sup>[2]</sup> To ensure

these characteristics, it is necessary to conduct the synthesis within the suitable concentration range—excessive concentrations may lead to the formation of polymeric aggregates, while inadequate concentrations may hinder the assembly process. Consequently, it is crucial to meticulously design the constituents to favor the formation of MOCs over extended frameworks. Despite the challenges in synthesis, MOCs offer significant advantages in terms of their solution processability. They are in general soluble in a range of solvents, including water, meaning that their solution properties can be studied using a range of techniques including NMR spectroscopy, mass spectrometry, and both absorption and emission spectrophotometry, and that detailed kinetic studies of guest capture and release are possible. Importantly, MOCs can be adapted to post-modification or post-assembly in the solid state and solution.<sup>[9]</sup> Attributed to their precisely-defined cavities, adaptable pore sizes, and numerous functionalities, MOCs have attracted increasing attention in numerous fields of research, including biomedical applications, molecular recognition, host–guest chemistries, stabilization of reactive species, catalysis, and separation.<sup>[10–13]</sup> Besides MOCs, dynamic porous organic cages (OCs) have been extensively studied in view of their ‘self-healing’ and ‘error correction’ characteristics.<sup>[14–20]</sup> Synthesis of OCs relies on thermodynamically driven reactions yielding in the formation of covalent, yet reversible bonds, which provides an effective strategy towards minimalization of structural defects.<sup>[21]</sup> Starting from precursors with functional groups, OCs with desired properties can be directly synthesized<sup>[22]</sup> or generated by exploiting post-synthetic strategies (PSS).<sup>[23]</sup> The latter is integral to improving the functionality of the original structures, making OCs invaluable for providing framework characteristics required to host various guest molecules, including artificial molecular machines.<sup>[24]</sup> Moreover, post-modifications are also an effective tool to improve the yield and solubility of OCs.<sup>[25]</sup> From a chemical and application point of view, this is an extremely important issue, given the presence of dynamic covalent bonds (e.g., imine or disulfide bonds) sometimes strongly susceptible to environmental changes.

A common and extremely important feature of MOCs and OCs is the presence of reversible bonds in the structure. This not only allows the tuning of the composition of the target MOCs/OCs, but also influences their encapsulation properties, i.e., regulates the probability of breaking apart when exposed to specific triggers (whether a chemical or

[\*] Dr. W. Drożdż, Prof. A. R. Stefankiewicz  
Faculty of Chemistry, Adam Mickiewicz University  
Uniwersytetu Poznańskiego 8, 61-614 Poznań (Poland)  
E-mail: ars@amu.edu.pl

Dr. W. Drożdż, Dr. A. Ciesielski, Prof. A. R. Stefankiewicz  
Center for Advanced Technology, Adam Mickiewicz University  
Uniwersytetu Poznańskiego 10, 61-614 Poznań (Poland)  
E-mail: ciesielski@unistra.fr

Dr. A. Ciesielski  
Institut de Science et d'Ingénierie Supramoléculaires, Université de  
Strasbourg & CNRS  
8 allée Gaspard Monge, 67000 Strasbourg (France)

© 2023 The Authors. Angewandte Chemie International Edition published by Wiley-VCH GmbH. This is an open access article under the terms of the Creative Commons Attribution License, which permits use, distribution and reproduction in any medium, provided the original work is properly cited.

physical stimulus) and the release of the guest molecule contained inside the cage. Despite many advantages of architectures exhibiting dynamic features at both supra- and molecular levels, there are some obstacles that impede their practical implementation. The primary constraint is their vulnerability to environmental conditions, which often restricts their stability. Additionally, their topology is another factor that hinders their ability to be widely applied. Despite having a three-dimensional shape with an accessible hollow internal cavity and very well-understood host–guest interactions, these systems possess a finite structure. To a large extent, this is a factor limiting the efficiency of the processes in which they participate, such as storage or transport. In this respect, porous networks like MOFs and COFs still lead the way.

Fortunately, recent progress in the field has made it possible to overcome these issues to a great extent. The ability to precisely control the shape and size of the cages' cavities, together with the possibility of outer-surface functionalization,<sup>[9,26]</sup> enables their incorporation on/into various platforms (e.g., surfaces or membranes), allowing the formation of functional hybrid structures.<sup>[6,27,28]</sup> Such approaches enhance the stability of cages, harness the emergence of new physicochemical properties and enhance the characteristics of the pristine components in a synergistic manner.<sup>[12,29–31]</sup> Through mastery of the principles of dynamic chemistry, different functional molecules have been utilized to produce cage-decorated materials exploiting notably different properties.

This Review discusses the progress made in the functionalization of various multidimensional systems (such as 0D

nanoparticles, 1D polymers, and 2D/3D materials) with dynamic cage-like architectures. To the best of our knowledge, there is no in-depth review discussing functionality-driven hybridization of dynamic cages with 0- to 3- dimensional materials. While thematically similar articles have been published, the vast majority focuses either on the cage design principles in terms of their structural properties,<sup>[5,22]</sup> functions<sup>[32]</sup> or (post-) modification methods, which in some cases lead to the desired functional materials.<sup>[9,26]</sup> Only a few review articles describing surface/interface modifications of a strictly defined group of materials with dynamic assemblies have been published so far, however they tend to focus on 1D polymers only.<sup>[6,33]</sup> In this Review, we focus on exploring the relationship between the properties of the cages and their structural features, as well as the types of functionalization applied to their outer surfaces. We also discuss the potential and drawbacks of cage-based systems applications highlighted in Figure 1. Preceded by an introduction on dynamic cage architectures in the context of smart materials, each of the consecutive sections is devoted to a different group of cage-decorated nanostructured materials, ranging from 0D to 3D systems.

## 2. Synthesis and Properties of Dynamic Cage Architectures—Importance in Terms of Smart Materials

Self-assembly is the most promising approach for the construction of functional nanostructures. It involves the



Wojciech Drożdż received his M.Sc. in Chemistry from the Adam Mickiewicz University in Poznań, Poland in 2015. The same year he joined the research group of Prof. Artur Stefankiewicz and worked towards his PhD (received in 2019) on the multi-dynamic molecular and supramolecular systems. His current research focuses on the design and synthesis of novel functional three-dimensional architectures based on reversible bonds.



Artur Ciesielski obtained his M.Sc. from Adam Mickiewicz University, followed by his PhD from the University of Strasbourg. In 2022, he became a CNRS research director at the Institut de Science et d'Ingénierie Supramoléculaires (ISIS). In 2018, he was appointed as visiting professor at the Centre for Advanced Technologies of Adam Mickiewicz University in Poznań (Poland). He is a board member of the Young Academy of Europe (YAE). His research interests include the design of supramolecular systems, self-assembly

of nanopatterns, and production and chemical modification of 2D materials towards applications in sensing and energy storage.



Artur R. Stefankiewicz is currently a Full Professor and Deputy Director of the Center for Advanced Technology at the Adam Mickiewicz University in Poznań. He received his Ph.D. in 2009 from the Université de Strasbourg (France) under the supervision of Prof. Jean-Marie Lehn. After four years of postdoctoral research with Prof. Jeremy K. M. Sanders at the University of Cambridge, he joined the Adam Mickiewicz University in Poznań (Poland) where he set up his independent research group. His research focuses on the areas of supramolecular, dynamic combinatorial/covalent chemistry, and the design and synthesis of novel functional nanostructures.

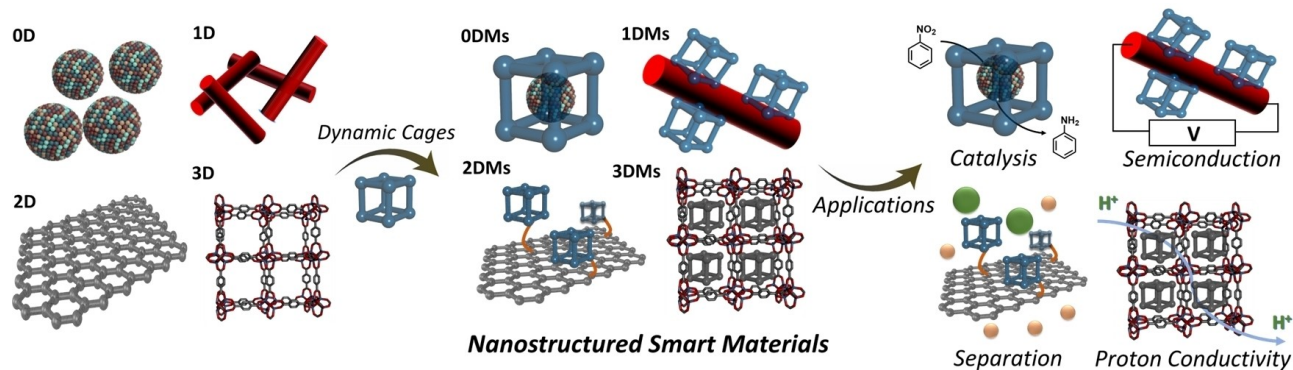


**Figure 1.** Overview of cage-decorated multidimensional materials (0–3DMs) with their possible functions described in this Review.

exploitation of labile interactions between kinetically inert molecular or ionic units to rapidly form their thermodynamically preferred (most stable) aggregate architectures. Together with a precise design of the building blocks, this approach provides access to a range of compounds with an enormous variety of forms such as macrocycles, cages, catenanes, and knots.<sup>[34–38]</sup> As part of functional self-assembled systems, dynamic covalent cage-like compounds have been the subject of intense research for both their unique structural features such as a hollow cavity, rigidity, and open pores that provide access to the external environment, but also numerous applications.<sup>[30,31]</sup>

The construction of such molecules varies depending on the type of dynamic linkage.<sup>[21]</sup> As an alternative to the more demanding synthesis of irreversible-covalent-bond cages, dynamic chemistry enables the construction of reversible covalent-bond cages from precisely chosen synthons. Using various dynamic covalent reactions including metathesis,<sup>[17,39,40]</sup> imine<sup>[41–47]</sup>/disulfide<sup>[48–52]</sup>/ester bond formation,<sup>[53,54]</sup> etc., organic cages with intrinsic properties have been successfully synthesized in high yields.<sup>[22]</sup> Regardless of the type of linkages, proper design of the components is a key step for the development of OCs. Choosing a functionalized organic linker with at least two binding units is crucial for the effectiveness of this process. Additionally, for the creation of a cage, the linker must have a geometry that corresponds with the second organic building block. Generally, as the angle of the linker becomes wider, the size of the cage tends to increase.<sup>[41]</sup> However, it should be kept in mind that even a small, undesirable change in the linker angle can have a drastic effect on the formation of OCs. Thus, to avoid unnecessary but costly experimental optimization processes, numerous computational tools can be used to predict the best approach for a given chemical reaction. These are mainly based on two solutions: force field methods and electronic structure calculations.<sup>[55–58]</sup>

An additional feature of OCs is the ability to generate more complex networks, by exploiting noncovalent intermolecular interactions between cages, typically through post-synthetic crystallization. The OC-based networks are characterized by high crystallinity, yet still exhibit rather poor stability, compared to framework materials (zeolites, covalent organic frameworks—COFs, MOFs, etc.).<sup>[59]</sup> One such

example has been demonstrated by Cooper et al., where they exploited the advantages of the dynamic nature of imine bond to obtain a tetrahedral molecule **OC-1** from an aromatic trialdehyde and ethylenediamine in ethyl acetate (EtOAc), as shown in Figure 2a.<sup>[60]</sup> The isolated cage exists as a solvate with 2.5 EtOAc solvent molecules. Thermal treatment to remove the solvent simultaneously alters the structure of the cage. The resulting solid polymorph **OC-1 $\alpha$** , as well as the solvate, are non-porous for gas molecules such as N<sub>2</sub> or H<sub>2</sub> at 77 K but exposure to dichloromethane (DCM) vapor and subsequent desolvation triggers another solid-state transformation to polymorph **OC-1 $\beta$** , that possess a 3D channel network (based on X-Ray Diffraction studies

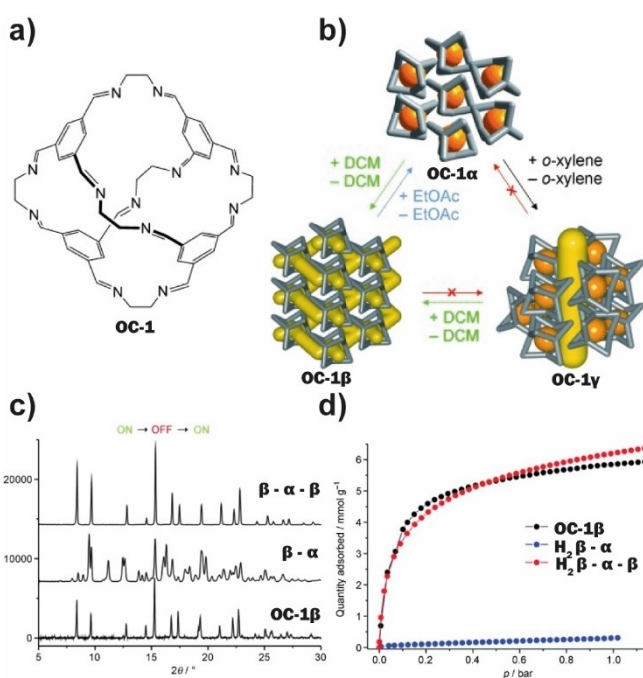


**Figure 2.** a) structure of a tetrahedral cage **OC-1**; b) solid-state transformation between different polymorphs (**OC-1 $\alpha$ - $\gamma$** ) upon treatment with appropriate solvents; c) PXRD of solid-state reversible polymorph conversion; d) H<sub>2</sub> adsorption isotherm at 77 K for reversible switching polymorphs. Reproduced from Ref. [60] with permission. Copyright 2011, WILEY-VCH.

—XRD). The switching between two polymorphs is fully reversible and is triggered by exposure to certain solvents (EtOAc for **OC-1 $\alpha$**  and DCM for **OC-1 $\beta$** ) followed by their removal (Figure 2c). Although polymorph **1 $\alpha$**  shows no adsorptive behavior, **OC-1 $\beta$**  shows selective encapsulation of H<sub>2</sub> at 5.9 mmol g<sup>-1</sup> H<sub>2</sub>, with no uptake of N<sub>2</sub> at all.

The absorption H<sub>2</sub> of can be reversibly controlled in “on-off-on” fashion with proper solvent treatment (Figure 2d). Interestingly, the use of *o*-xylene solvent in the synthetic procedure leads to the formation of yet another polymorph **OC-1 $\gamma$** , porous to both N<sub>2</sub> and H<sub>2</sub>, but its structure is not transformed when the two previously mentioned solvents are added (Figure 2b).

Later on, the same group also investigated the selective guest encapsulation by a series of imine-based porous OCs obtained from trialdehydes and 1,2-substituted diamines.<sup>[61]</sup> During vapor adsorption studies, they found that the well-known solid OC composed of 1,3,5-triformylbenzene and (1R, 2R)-cyclohexane-substituted diamine, showed good selectivity towards 4-ethyltoluene with no absorption of its isomer mesitylene. Given the similar molecular volumes of the two aromatics, the difference in affinity can be ascribed predominantly to the guest shape, rather than to size. With this in mind, a cage-decorated chromatographic column was prepared for the dynamic separation of isomers. The chromatograms obtained showed the presence of mesitylene almost immediately after pumping onto the bed, while 4-ethyltoluene remained adsorbed on the resin.

Synthesis of supramolecular cages requires meticulous design of organic ligands suited to interacting via non-covalent interactions such as hydrogen- or halogen bonds, or coordination with metal ions. The latter are of particular importance due to their relatively high stability in a range of solvents (from polar to non-polar) and ease of functionalization.<sup>[62,63]</sup> Most of MOCs rely on straightforward solution-based procedures, where the building blocks are mixed at elevated temperatures. When the components are well-designed, the collaborative process of assembly frequently results in the quantitative formation of the desired product. The MOC/OC assembly process can be significantly hindered by even the slightest alterations in synthetic conditions such as changes in the solvent, counterion type or concentration. Depending on the target use of the cage, it can be modified as desired. Noteworthy, the presence of functional groups in the scaffold of the cage directly translates into its overall properties. Functional groups can be introduced in two ways: during the ligand synthesis followed by the assembly of the cage, or through post-synthetic modification of an already obtained MOC.<sup>[26]</sup>

So far, MOCs have been subjected to numerous functionalizations that enable selective detection of analytes (fluorescent sensors),<sup>[64,65]</sup> binding/separation of particles with various sizes (size selective host–guest system),<sup>[33,66,67]</sup> conducting catalytic reactions (catalysts, nanoreactors)<sup>[68,69]</sup> or a change in solubility (tailorable systems).<sup>[32]</sup> Like supramolecular cages, covalent cages may also undergo structural modifications so as to impart the newly obtained architecture desired properties (porous solid and liquid, molecular flask). Due to the, in practice, reversible nature of

the employed covalent/coordination bonds, dynamic cages can deform or de-ligate, to encapsulate a guest much larger than the cage pores. Although different types of functional materials with internal voids are known (e.g., MOFs, COFs, zeolites), they possess several limitations including low solubility (or even dispersibility) if their use in homogeneous catalysis is desired, harsh synthesis reaction conditions or non-adaptable structures.

Nonetheless, these structures also exhibit numerous positive features that grasp the interest of researchers, despite the aforementioned drawbacks. MOFs, similar to structures discussed in this Review, exhibit several important properties that affect their application potential. They are characterized by rather good stability, with an increasing number of water-stable MOFs, high crystallinity as well as excellent designability. The field of smart materials based on self-assembled cage systems is still in its infancy with not as many examples as other solid porous materials. However, thanks to their unique properties like good solubility in a range of solvents (depending on the structure of the cage) and resulting ability to functionalization through the post-modification protocol, they are considered a perfect mean to overcome the drawbacks of less processable solids and reduce the cost of production of fine nanostructured materials and improve the efficiency of the processes in which they will be utilized. The multitude of cage architectures obtained so far, both MOCs and OCs, makes it impossible to determine in a simple and transparent way their basic parameters, such as susceptibility to environmental conditions, stability in the reaction medium, thermal resistance, or ability to encapsulate guest molecules. These are strictly individual characteristics for each MOC/OC system, and the selection of one of them for the creation of nanostructured materials must be preceded by a full and thorough analysis of each cage individually. However, it should be remembered that they are reversible systems, and while their stability may be enhanced to some extent as a result of embedding onto/into the substrate, they can still disassemble under unfavorable conditions (specific to the cage type).

### 3. Dynamic Cage Hybrids and Composites as Smart Materials

The following section is focused on an in-depth presentation of dynamic-cage decorated functional materials with different topologies, ranging from 0 to 3-dimensional. Examples of 0D materials are mainly represented by spherical metal/semi-metal nanoparticles which, due to their size and interesting physicochemical properties, are an excellent material for interactions with cage-type systems. On the other hand, 1D materials are characterized by a rather linear topologies often exhibiting high surface areas (polymers). While 2DMs are nanostructures obtained by embedding cages on highly oriented surfaces like graphene, gold or silica, 3D systems are characterized by the presence of cages incorporated into the cavities of already existing 3D

structures like MOFs. More detailed information on each of these types will be presented in individual section of the article. Moreover, both methods of deposition of reversible coordination and/or covalent systems onto/into chosen materials as well as their influence on the physicochemical properties of the resulting nanostructures are thoroughly described. Cage-based materials generated by such an approach are characterized by often better (composites) or even completely new physicochemical properties (hybrids) compared to their building components and can be successfully used in a wide range of processes such as heterogeneous catalysis, separation of gases, or chiral particles, proton and electron transfer or host-guest binding of various analytes.

### 3.1. 0D Material-Based Hybrids and Composites

0-dimensional materials (ODMs) constitute a wide variety of systems including quantum dots (QDs),<sup>[70–73]</sup> fullerenes,<sup>[74,75]</sup> metal nanoparticles (NPs),<sup>[76,77]</sup> polymer dots (Pdots).<sup>[78,79]</sup> Benefiting from their ultra-small size and high surface-to-volume ratios, ODMs have found their use in ion and pathogen detection, biomolecular recognition as well as in the diagnosis of various diseases.<sup>[80]</sup> Compared to bulk high-dimensional nanomaterials, ODMs are mostly spherical or quasi-spherical with a diameter < 100 nm. However, their remarkable properties are not due to the available empty cavities (as in the case of cages of similar size) but rather due to the possible surface interactions with other molecules. The functionalization of ODMs with appropriate (supra)molecular receptors can impart new physicochemical properties.<sup>[81,82]</sup> An excellent example of the fabrication of ODM-based composites with cages is the work of Kang et al. concerning the functionalization of mesoporous silica with a cavity size of ~6 nm and a pore entrance of ~2 nm (commercially available silica named **SBA-16**) with cuboctahedral **MOC-1** synthesized from  $\text{Cu}(\text{NO}_3)_2$  and the organic ligand 5-sulfonato-1,3-benzenedicarboxylate.<sup>[83]</sup> **MOC-1** was successfully incorporated into the cavity of mesoporous silica using a double-solvent strategy. First, precursors of the MOC were dissolved in a small volume of methanol, then added to a hexane solution of **SBA-16**. Due to the hydrophilic character of the inner surface of silica, the polar solvent migrated through its pores by capillary action. Subsequent addition of the initiator (2,6-lutidine) led to the formation of MOC@silica nanocomposites, as shown in Figure 3a. Interestingly, with different amounts of the precursors, either one or two cages could be formed within each cavity, giving **MOC-1/SBA-16** and **MOC-1''/SBA-16** respectively. Several analytical methods confirmed the structure of the obtained materials, including scanning transmission electron microscopy (STEM), absorption spectroscopy, and powder X-Ray diffraction (PXRD). An important feature of the composites was the uniform dispersion of MOCs in the pores **SBA-16**. This resulted in good uptake of gas molecules, carbon dioxide ( $\text{CO}_2$ ) and propene ( $\text{C}_3\text{H}_6$ ), while the cages themselves formed non-porous solids with negligible sorption properties. The latter

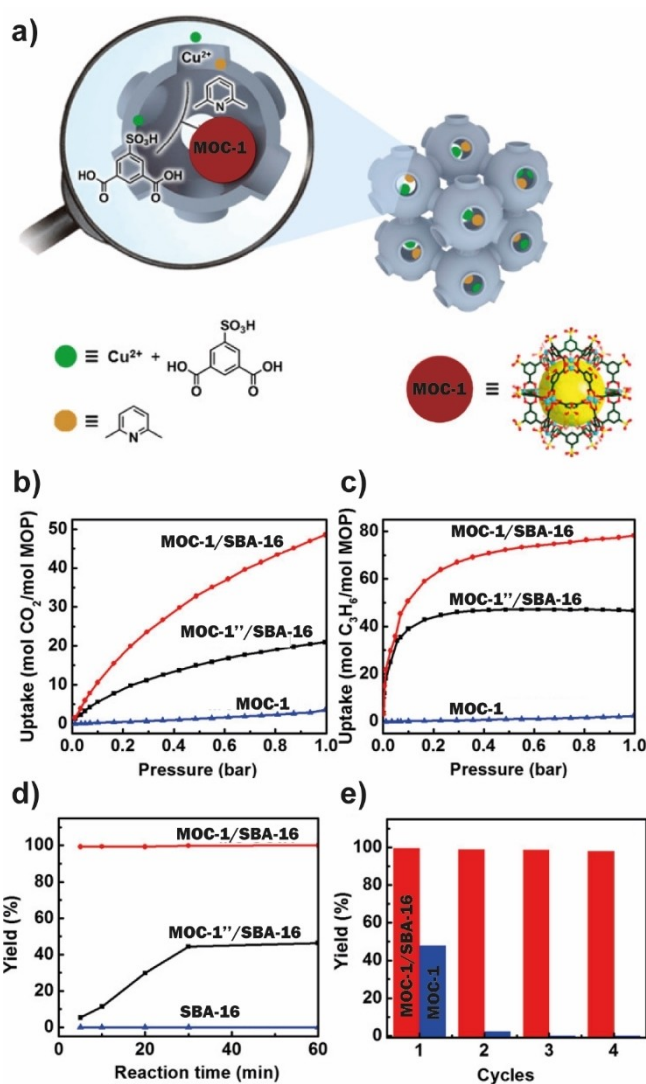


**Figure 3.** a) Schematic diagram for the decoration of mesoporous **SBA-16** with **MOC-1**; b,c) absorption isotherm of  $\text{CO}_2$  and  $\text{C}_3\text{H}_6$  at 273 K, respectively; d) catalytic performance of the ring-opening reaction in styrene oxide; e) reusability of **MOC-1/SBA-16** and **MOC-1** in a catalytic reaction. Reproduced from Ref. [83] with permission. Copyright 2016, American Chemical Society.

were due to the blockage of the internal spaces of the cages as a result of their aggregation. Thus, in **MOC-1/SBA-16** composite, the  $\text{CO}_2$  uptake reached 48 mol  $\text{CO}_2$  per 1 mol of **MOC-1**, while in **MOC-1''/SBA-16** uptake was almost two times lower, confirming the hypothesis that cage aggregation may block access to its interior. Similar results were obtained with  $\text{C}_3\text{H}_6$ , where the uptake of **MOC-1/SBA-16** was 78 mol  $\text{CO}_2$ /mol MOC (Figure 3b,c). Due to the presence of a coordinatively unsaturated metal active site, the MOC@silica composite can also serve as a catalyst in ring-opening reactions. The catalytic conversion of styrene oxide to 2-methoxy-2-phenylethanol on **MOC-1/SBA-16** proceeded with an efficiency of almost 100 %, compared to 0 % for pristine **SBA-16** and 48 % for bulk **MOC-1** (Figure 3d). Further advantages were observed concerning

reusability of the catalysts. As shown in Figure 3e, the activity of the composite does not decrease even after 4 catalytic cycles, while the conversion of styrene in the non-incorporated cage system drops to nearly 2% after only the second cycle.

Another interesting application of silica in the creation of 0DM is the functionalization of capillary columns with chiral MOCs. In this regard, the group of Yuan developed chiral stationary phases using a dynamic coating approach.<sup>[84]</sup> Three different Schiff-based chiral cages were used in the successful preparation of MOC-coated open-tubular columns. The latter showed good enantiomeric recognition ability towards chiral amine, acid, alcohol, and ketone compounds. Additionally, MOC obtained upon reaction of  $\text{Zn}^{2+}$  salt with enantiopure (1R,2R)-diaminocyclohexane and 4-*tert*-butyl-2,6-diformylphenol has also been employed in capillary treatment, leading to the preparation of homo-chiral columns for gas separation,<sup>[85]</sup> as well as of a novel stereoselective stationary phase with poly-(ionic liquid-co-ethylene dimethacrylate) for the purposes of capillary electrochromatography in selective separation of mandelic acid, benzoin and furoin enantiomers and nitrocompounds.<sup>[86]</sup>

As well as silica, gold nanoparticles (Au NPs) have also been successfully used in the formation of 0D cage-decorated nanocomposites. Li and co-workers introduced a multi-step procedure to construct a MOC-decorated plasmonic composite with sensing properties.<sup>[87]</sup> A Cu-based MOC was first prepared by reacting  $\text{Cu}_2(\text{OAc})_4$  with a ditopic organic ligand giving an unbound amino group. Immersion of the Au-NPs surface-functionalized with 4-mercaptopyridine in a solution of cage resulted in the formation of the desired MOC-decorated material through the coordination between axial Cu sites of the cage and pyridine moieties of the Au surface. To assess the sensing properties, the generated 0DM was exposed to solutions of nitro-explosives at various concentrations and the results were validated through surface-enhanced Raman spectroscopy (SERS). Due to the presence of electron-donating  $\text{NH}_2$  group and the unsaturated  $\text{Cu}^{2+}$  metal sites, multiple interactions with guest molecules were possible to form, including charge-transfer and Bronsted acid-base interactions, significantly strengthening the association of host-guest complex. In depth studies revealed impressive detection limits for explosives at concentrations as low as  $10^{-11}$  M for trinitrotoluene (TNT) and hexogen (RDX), and  $10^{-9}$  M for octogen (HMX). The aforementioned SERS technique has also been successfully used for the characterization of Pd-based MOC with a phenothiazine backbone upon their adsorption on an Au surface.<sup>[88]</sup>

Recent work published in collaboration between Stang, Sessler, and Li, describes a novel use of highly oriented pyrolytic graphite surfaces (HOPG) in the formation of 1D nanowires by metallo-supramolecular cuboctahedra.<sup>[89]</sup> A MOC architecture was first synthesized through a reaction between a bent di-Pt unit and a Zn-coordinated porphyrin-based ligand. Given the well-known ability of porphyrins to interact with each other, the authors examined the stacking pattern on HOPG. Surprisingly, instead of the expected 2D

monolayer of MOC, double-helical nanowires with uniform diameter and ultralong length were obtained through the drop-casting method with an incubation time lower than 30 s. Additional experiments confirmed conductivity of a generated device when deposited on a substrate like  $\text{SiO}_2/\text{Si}$  with Au/Cr contacts. Importantly, this property was not obverted for both isolated and HOPG-deposited nanowires. Conductivity curves obtained at different applied voltages showed high stability of the nanowire (stable at 20 V). With the average resistance at  $6.7 \pm 1.2 \text{ G}\Omega$ , the obtained material has been characterized as a p-type semiconductor.

Ryan et al. focused on a 0D material based on the fabrication of alumina with two distinct, Fe-MOCs composed of  $C_3$ -symmetric ligand based on triazine moiety<sup>[90]</sup> or ditopic ligand with 4,4'-diaminobiphenyl-2,2'-disulfonic acid component.<sup>[91]</sup> In this regard, authors performed the adsorption of self-assembled tetrahedral anionic and cationic cages on acidic and basic alumina, respectively.<sup>[92]</sup> The obtained materials exhibited the ability to bind fluorobenzene derivatives with the possibility of their subsequent release after washing with DCM. Additional studies of guest displacement showed the applicability of the system in Diels–Alder reaction. While alumina columns with anionic MOC were able to stabilize an otherwise unstable cyclopentadiene, the cationic counterpart showed good affinity towards N-propyl maleimide. Subsequent washing of columns with DCM resulted in the release of both guests' molecules and the formation of Diels–Alder product when combined.

A different approach has been presented by Jiang et al. who exploited the dynamic OCs as both templating and stabilizing agents for production of metallic NPs. In this case, the imine-based OC was not deposited on the surface of NPs but rather served as a host for  $\text{Pd}^{2+}$  ions, reduced in  $\text{H}_2$  to ultra-small metal NPs. Admittedly, the resulting NPs@OC exhibited slightly lower Brunauer–Emmett–Teller (BET) surface area ( $350 \text{ m}^2 \text{ g}^{-1}$ ) and  $\text{N}_2$  adsorption ( $4.7 \text{ mmol g}^{-1} \text{ N}_2$  at 77 K) in comparison to pristine OC ( $400 \text{ m}^2 \text{ g}^{-1}$  and  $5.5 \text{ mmol g}^{-1} \text{ N}_2$ , respectively) but exhibited catalytic activity toward CO oxidation.<sup>[93]</sup>

Similarly, Sun et al. showed the formation of metal NPs inside benzothiadiazole-based imine OC upon the reduction of  $\text{Pd}^{2+}$  ions. Due to the presence of photocatalytic organic moiety constituting the skeleton of the cage, obtained hybrid material exhibited high-yielding catalytic sequential hydroxylation of 4-nitrophenylboronic acid, followed by its reduction to 4-aminophenol. Interestingly, no final product was obtained when Pd/C catalyst was used, and only trace amounts were detected with isolated OC as catalyst.<sup>[94]</sup>

On the other hand, Hang and co-workers presented the location-controlled synthesis of Au NPs inside of thiacalixarene-based Co-MOC. The concentration dependent process allowed to obtain ultrafine metal NPs with 1.3 nm size inside the cavity of the cage with a low concentration of Au precursor and 4.7 nm NPs located on cage periphery. As obtained material allowed for homogeneous hydrogenation of 4-nitrophenol in methanol-DCM solvent mixture as well as catalytic decomposition of organic dyes: Congo red and methyl orange. The reaction with the latter resulted in a

complete reduction to colorless products within 75 seconds and 90 seconds, respectively.<sup>[95]</sup>

An interesting feature of dynamic OCs is their ability to form liquids with permanent porosity. This can be achieved, among other things, by using a solvent whose molecular size is too large to be able to fit inside the capsule cavity. The basic set of properties of these materials is their simultaneous fluidity, porosity and tunability, which can be easily adapted for facile industrial-scale implementation. So far, they have been shown to have a great potential for use in gas storage, separation and even catalysis.<sup>[96–99]</sup> The term porous liquid was initially coined by James and co-authors, who suggested the existence of three types of liquid materials.<sup>[100]</sup> *Type I* are neat liquids made up only of molecules possessing an internal cavity, exhibiting rigidity to avoid collapsing and preventing the cavity from self-filling. *Type II* refers to systems in which a host with a defined cavity size is dissolved in a solvent that has no affinity for the host cavity. *Type III* are porous liquids—framework materials obtained through the dispersion in a suitable solvent. Since then, numerous porous liquid materials have been developed based on hollow carbon spheres,<sup>[101]</sup> externally functionalized silica spheres,<sup>[102]</sup> metal–organic frameworks,<sup>[103,104]</sup> liquid coordination polymers<sup>[103]</sup> and many others,<sup>[105–107]</sup> and have found application mainly in gas separation/storage. However, in the context of smart materials, an important achievement is the work of the Nitschke group, who published a *Type I* porous liquid based on MOC with a terminally incorporated poly(ethylene glycol) (PEG)-imidazolium chain.<sup>[108]</sup> Tetrahedral **MOCs-2a–c** were obtained upon reaction of trialdehyde **A** with anilines functionalized with different lengths of PEG chains (**B,C**) or methyl groups for comparison, and a  $Zn^{2+}$  salt in acetonitrile ( $CH_3CN$ ) under microwave conditions (Figure 4a). Interestingly, **MOC-2c** with a short pentaethylene glycol chain was a solid material, while longer chains were necessary to lower the melting point of the **MOC-2b** below room temperature. Oscillatory-dependent rheological studies confirmed a liquid behavior of the cage even with a dramatic decrease of the  $G'$  value (storage modulus). Moreover, temperature-dependent measurements established its liquid nature in the temperature range from 20 to 100 °C, along with an inversely proportional change in viscosity. This cage has an average void diameter of 6.29 Å calculated with the aid of positron annihilation lifetime spectroscopy. Such a value allows it to incorporate guests of various sizes. NMR measurements revealed a greater affinity for branched alcohols in comparison to linear, as a result of its selective size and shape complementarity. More importantly, **MOC-2b** also exhibited host–guest properties toward some of the most strongly ozone-depleting agents—chlorofluorocarbons (CFCs). Exposure of a deuterated acetonitrile ( $CD_3CN$ ) solution of **MOC-2b** to the gaseous CFCs: trichlorofluoromethane ( $CFCl_3$ ), dichlorodifluoromethane ( $CF_2Cl_2$ ) and chlorotrifluoromethane ( $CF_3Cl$ ) (Figure 4b) resulted, as shown by the up-field shift of the CFC  $^{19}F$  NMR signals, in successful encapsulation of the guests. Due to the negligible vapour pressure of the **MOC-2b**, all guest encapsulation processes

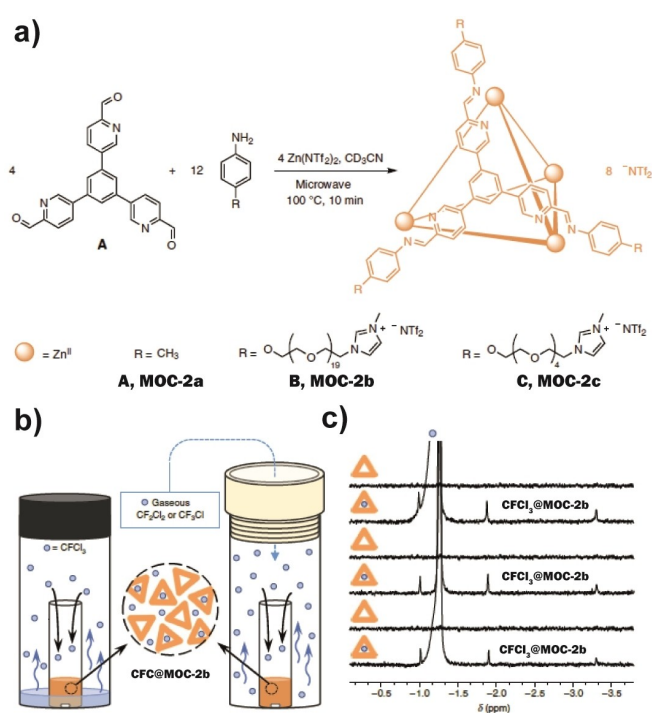


**Figure 4.** a) Synthesis of porous ionic liquid tetrahedral **MOC-2a–c** from substituted amines (**A–C**) and tripodal aldehyde in the presence of  $Zn^{II}$  salt; b) schematic uptake of gaseous guest molecules by liquid **MOC-2b**; c) reversible guest uptake–release observed by  $^{19}F$  NMR spectroscopy. Reproduced from Ref. [108] with permission. Copyright 2020, Nature Chemistry.

were reversible, and the guests could be removed from the cage under reduced pressure, as shown in Figure 4c.

Recently, the same group invented a MOC-based liquid membrane as an intelligent device for the selective transport of hydrocarbons.<sup>[109]</sup> Aqueous solutions of previously obtained  $Fe^{2+}$  and  $Co^{2+}$  cages showed good cargo properties, driven by the guest binding affinity. This example represents one of many possible solutions in which, through the appropriate choice of water-soluble cages, both the shape and size of the encapsulated guest can be controlled, thereby meeting the requirements of novel material separation purposes.

Other interesting results have been presented by Ganta et al., where a banana-shaped  $Pd^{2+}$  cage functionalized with cholesterol groups, was successfully used for the generation of 0D nonaqueous, oil-in-oil (o/o) reactive emulsions by mixing dimethylsulfoxide (DMSO) and nonpolar solvents like octane, hexane, cyclohexane and various others.<sup>[110]</sup> While the cationic skeleton of the cage acts as a hydrophilic head, the cholesterol moiety constitutes a non-polar tail, thus imitating a typical surface-active agent. Further studies showed the good catalytic potential of such o/o emulsions in the formation of polyurethanes and polyurea, preventing the violent reaction of isocyanates with water. The same group also described an o/o emulsion containing a heteroleptic cage suitable for the synthesis of spherical metal oxide macrocapsules from water-sensitive substrates.<sup>[111]</sup>

In 2015, Cooper, James, and co-workers designed porous liquids of *Type II*.<sup>[106]</sup> Imine-based OCs were successfully synthesized from tribenzaldehyde and crown ether-functionalized diamine compounds in chloroform solution. To obtain a porous material, the designed cage was dissolved in a non-intercalating solvent: 15-crown-5 ether. Functionalization with its ether ring enabled the cage to dissolve in the solvent at a high concentration (44 wt%). With an internal cavity of 5 Å diameter and an access window of 4 Å, the OC showed potential use for gas storage due to its good affinity for methane. While methane solubility in pure 15-crown-5 at 30 °C was found to be  $6.7 \mu\text{mol g}^{-1}$ , its solubility increased nearly eightfold ( $52 \mu\text{mol g}^{-1}$ ) in the porous liquids.

The examples examined in this section demonstrate the advantages that arise from pairing 0D nanoparticles with dynamic cages. The resulting materials display greatly enhanced properties in areas such as catalytic activity in epoxide ring-opening reactions, gas absorption, detection limits for hazardous substances, as well as chiral separation and encapsulation of freons. Despite the significant advances made in the creation of 0D cage hybrids and composites, there remains ample room for improvement in synthetic procedures, in order to achieve even greater efficiency, flawless structures, and improved stability of these materials.

### 3.2. 1D Materials

One-dimensional materials (1DMs), including polymers, nanotubes (NTs), nanofibres, and nanowires (NWs), have attracted much attention due to their interesting physicochemical properties (e.g., linear morphology, large surface area, many accessible active sites), and wide range of potential applications as semiconductors, permeable materials or energy conversion and storage devices.<sup>[112–115]</sup> 1DMs can also exhibit a multitude of distinct characteristics (e.g., hydrophilicity or electrochemical properties), depending on their composition and structure, leading to essentially unlimited possibilities for the rational design of functional materials. In this regard, the hybridization of 1DMs with dynamic assemblies is of extreme importance, considering the possible beneficial outcome of the process.

For decades, linear polymers of varying compositions have constituted an interesting group of 1DMs. Their unique structure-dependent physicochemical properties like mechanical strength, wide compositional diversity, permanent porosity, and convenient processability allow for applications in various fields such as industrial separation, optoelectronic devices, or molecular transport. So far, several strategies have been developed to tune polymer structure to produce desirable properties. In terms of cage-decorated 1D polymers, two main groups can be distinguished. The first one is represented by polymer membranes (mixed-matrix materials—MMMs) with both OCs or MOCs embedded inside the structure of the polymer.<sup>[116]</sup> The good solubility of the vast majority of finite systems like dynamic MOCs in common solvents most frequently leads to controllable dispersion in the derived MMMs and thus limits the formation of nonselective voids or interfacial defects. More-

over, the addition of the porous molecules in the polymeric matrix promotes both diffusivity and solubility of the generated 1DM. Such designed and synthesized cage-embedded 1DMs with uniform morphology have been extensively investigated in separation processes. The ability to modulate the cavity of the cage by precise design of the ligand's backbone allows for size-selective encapsulation or transport of a desired guest from any mixture of analytes through the permeable membrane.

In this regard, many MMMs with porous MOCs have been designed and successfully used, mainly in transport/separation processes. For example, Liu et al. exploited MOC with the formula  $\text{Cu}_{24}(\text{NH}_2\text{-mBDC})_{24}$  (mBDC = 5-amino-1,3 benzenedicarboxylate) as a filler in polymer matrix, which resulted in a series of membranes with different loading.<sup>[117]</sup> When compared to the neat polymer, the best permeability, selectivity, and aging resistance was achieved for the membrane needing only 1.6 wt% MOC loading. The 1DMs exhibited increased permeability for  $\text{CO}_2$  (1413 Barrer) and modest improvement of selectivity in  $\text{CO}_2/\text{N}_2$  system (26.7) when compared to non-functionalized polymer (1010 Barrer and 23.9, respectively). Such a low concentration of the cage in membrane additionally prevented agglomeration of the MOC and provided good dispersion throughout the membrane. Further, increase in loading did not result in the enhancement of uptake properties.

Similarly, Perez et al. focused on the functionalization of the commercially available polymer Matrimid<sup>®</sup> with Cu-based MOC for application in gas separation.<sup>[118]</sup> MOC was generated by coordination of 5-dodecoxyisophthalic acid to  $\text{Cu}(\text{AcOEt})_2$ , and exhibited good solubility in organic solvents. The latter feature allowed the target 1DMs to be obtained with a wide range of additive loading, from 16 to 80 wt%. The presence of long alkyl chains in the structure of the MOC effectively inhibited the aggregation process, leading to good dispersion in the polymer matrix. The newly obtained MMMs exhibited a significant enhancement in gas sorption by approximately 5.2 mmol/g compared to the pristine polymer matrix. The increase of the  $\text{CO}_2$  sorption by 23 wt%-MMM at pressures above 30 bar at two different temperatures (35 °C, 70 °C) indicated flexibility of the MOCs, leading to the opening of their pores. Interestingly, neither the cage itself nor the prepared 1DM showed any sorption capacities for hydrogen ( $\text{H}_2$ ) and methane ( $\text{CH}_4$ ) due to the oxygen-induced hydrophilicity of the linker in the MOC pore aperture. Furthermore, the non-polar alkyl chain directly affected the permeability of the MMM for more condensable gases, like  $\text{CH}_4$ ,  $\text{C}_3\text{H}_6$  or  $\text{C}_3\text{H}_8$  (propane), with increased loading of MOC above 33 wt%. No significant improvement in permeability was observed for  $\text{H}_2$ ,  $\text{N}_2$ ,  $\text{CO}_2$ , or  $\text{O}_2$  at higher concentrations of cage in the polymer.

The same cage system has been exploited in the formation of synthetic ion channels in bilayer lipid membranes. The large MOC cavity with a diameter of  $\approx 14$  Å allowed for efficient proton and alkali metal transport.<sup>[119]</sup>

Other Cu-MOCs have also been used for the formation of MMMs with effective gas separation properties.<sup>[120]</sup> They include the hydrophilic cages with attached PEG groups combined with cross-linked polyethylene oxide,<sup>[121]</sup> or sulfo-

nated ones serving as a filler in polysulfone matrix.<sup>[122]</sup> Both MMMs benefit from uniform dispersion of the MOCs and diverse loading, leading to good permeability and separation factors for CO<sub>2</sub> over the other gas molecules. Additionally, Zhao et al. have described a soluble Cu-MOC based on 5-*t*-butyl-1,3-benzenedicarboxylic acid as a filler in the hyper-branched polymer Boltorn W3000.<sup>[123]</sup> The target 1DM was obtained by an immersion-coating method, with cage loadings between 1.6–13 wt%. Pervaporation studies for a toluene/*n*-heptane mixture showed enhanced separation factors and permeate fluxes for the fabricated polymer (19 and 220.5 g m<sup>-2</sup> h<sup>-1</sup>) in comparison to pure W3000 membrane (5.9 and 50 g m<sup>-2</sup> h<sup>-1</sup>, respectively). In continuation, Zhao et al. examined the effect of the substituent in the linker of the MOC on the properties of the obtained MMMs.<sup>[124]</sup> For this purpose, they used cage molecules containing different functional groups: -SO<sub>3</sub>Na<sub>n</sub>H<sub>m</sub>, -OH, and -*t*Bu, as fillers in the polymers W3000. Although all materials showed good filler dispersion and improved pervaporation separation toward aromatic/aliphatic mixtures in comparison to the pure polymer, the best adsorption properties of aromatic hydrocarbons were shown by the most polar, sulfonated MMM.

Besides Cu-based MOCs, Rh-MOCs have also been successfully used in the fabrication of polymers for molecular separation and gas separation.<sup>[125]</sup> Using the Langmuir–Blodgett technique, Andrés et al. achieved the synthesis of 1DM from a Rh-MOC composed of 5-dodecoxybenzene-1,3-dicarboxylate, Rh–Rh paddlewheel unite and the permeable polymer poly[1-(trimethylsilyl)-1-propyne] (PTMSP). Functionalization of this MOC with long aliphatic chains allowed assembly of homogeneous 2–3 nm thick monolayer films at the air–water interface in the first step, followed by incorporation into the PTMSP. This membrane exhibited increased CO<sub>2</sub>/N<sub>2</sub> selectivity from 4.1 to 10.1 in comparison to the pristine polymer, while keeping a high CO<sub>2</sub> permeance.

The same polymer has been used for the formation of anti-ageing intercalated membranes with several types of MOCs varying in external organic chain length.<sup>[126]</sup>

An interesting example of MMM was described by Bushell et al., focusing on the previously described organic cage. In situ crystallization of the porous imine cage enabled formation of a dispersed phase of the targeted MMM with an amorphous glassy organic polymer matrix. This MMM showed enhanced permeability toward CO<sub>2</sub> and N<sub>2</sub> gases in comparison to both the pristine cage, and reduced derivative of this structure embedded in matrix. This was attributed to an amorphous structure of the much less rigid dodecamine cage without permanent porosity features in the solid state.<sup>[127]</sup>

The second type of functional 1D polymer is based on crosslinking of individual cage units. This type of material can be obtained using either an organic linker attached to the properly functionalized scaffold of the MOC or through the use of polymeric, flexible ligands, and cages as junctions. These strategies very often lead to the formation of a gel-like materials with interesting properties. The ability of such gels to trap large numbers of molecules within the cavity of

a cage makes them useful for applications that include drug delivery or catalysis. Furthermore, the dynamic nature of the linkages in these systems gives rise to useful 1DMs with self-healing, shear thinning, mechanoresponsive, stimuli-responsive, and many other properties.<sup>[128–130]</sup>

In this regard, Yuan et al. prepared the amine-functionalized Zr-MOC, further used for the fabrication of homoporous membranes through in situ cross-linking polymerization with poly(ethylene glycol) diacrylate (PEGDA) and poly(ethylene glycol) methyl ether acrylate (PEGMEA).<sup>[131]</sup> The 1DM obtained featured good solubility and thermal stability. Moreover, gas separation studies revealed good selectivity in CO<sub>2</sub>/CH<sub>4</sub> separation.

The same cage has been investigated by the Guo et al., where the targeted polyamide thin film nanocomposite (TFN) was synthesized with trimesoyl chloride as a cross-linking agent.<sup>[132]</sup> The network obtained not only exhibited excellent water permeance of 82.0 L·m<sup>-2</sup>·h<sup>-1</sup>·bar<sup>-1</sup>, but also selectively transported mono- and -divalent salt ions rejecting larger dye molecules.

Recently, Liu and co-authors described the formation of hyper-cross-linked metal polyhedra using Zr-MOCs.<sup>[133]</sup> A zirconium salt and organic linkers, 2-aminoterephthalic acid or 3,3-diamino-1,1-biphenyl-4,4-dicarboxylic acid, were used to obtain two separate MOCs, with terephthalaldehyde as linking agent. Due to the dynamic nature of the imine bond in the membranes formed, the resulting material offered enhanced mechanical properties, like resistance to breaking upon bending, twisting, or stretching when dry, or reshaping ability derived from the water-induced malleability when wet.

Another covalently-linked Zr-MOC based polymer has been described by Nam et al.<sup>[134]</sup> In this work, post-synthetic condensation between an amine group of the cage and acyl chloride linkers led to the formation of a polyMOC with retained porosity and crystallinity.

Quite a large group of cross-linked materials are represented by Pd-MOCs, where metal ions are coordinated by ditopic ligands having pyridine-N donors.<sup>[135–137]</sup> While the backbone of the ligand is specific for each purpose, the square planar geometry of the Pd complex remains crucial for the formation of dynamic MOCs of the general formula M<sub>n</sub>L<sub>2n</sub> (where M stand as metal ion and L as organic ligand). Although obtained 1D polymers have not been tested in terms of application, it has been shown that small ligand modifications can lead to quite significant changes of micro- and mesoscopic structures as well as interesting mechanical properties of the obtained polymers.

An interesting example of the formation of MOC-crosslinked polymers has been presented by the group of Johnson.<sup>[138]</sup> With the presence of two photoswitchable bis-pyridyl dithienylethene (DTE) groups connected with poly(ethyleneglycol) units in the structure of the ligand, new photoreversible Pd-based polyMOCs (**o-c-MOC-3**) were obtained. Upon irradiation with UV light, the open form of the DTE-ligand undergoes transformation to a closed one (Figure 5a *top* and *bottom*, respectively). The process was fully reversible upon treatment with green light, yet directly affected the topologies of the MOCs. While the open form

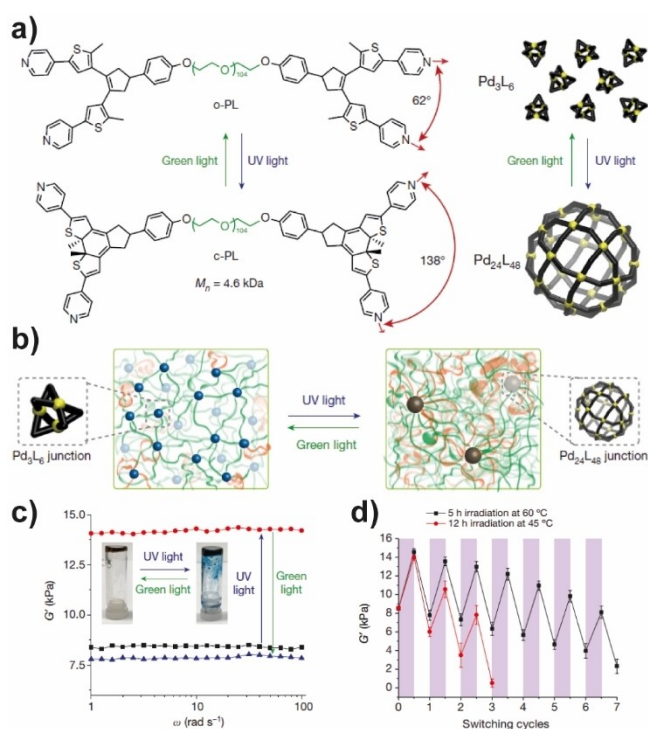


**Figure 5.** a) Chemical structures of a switchable ligand upon light stimuli with the corresponding MOCs-3 formed; b) photo-regulated interconversion of two networks' topologies; c) reversible conversion between o-MOC-3 and c-MOC-3 with the corresponding shear storage modulus ( $G'$ ); d) the correlation between irradiation time and shear modulus ( $G'$ ) value upon multiple topology switching. Reproduced from Ref. [138] with permission. Copyright 2018, Nature.

has smaller  $Pd_3L_6$  junctions, the closed involves the formation of much larger  $Pd_{24}L_{48}$  rhombicuboctahedra units (Figure 5a). Due to the polymeric nature of the ligand (bis-ditopic with PEG linker), reaction with 1 equiv. of  $Pd(CH_3CN)_4(BF_4)_2$  leads to the formation of o-MOC-3 gel, as shown in Figure 5b, left. This material exhibited elastic behavior with a storage modulus ( $G'$ ) of about 8.3 kPa at  $10 \text{ rad s}^{-1}$ . The irradiation of the o-MOC-3 with UV light induced topological changes of the polymer upon formation of c-MOC-3 gel, with an almost double  $G'$  factor. This was attributed to the presence of a greater number of defects in polymer networks, characteristic for 1DM with a higher-branched functionality  $f$  (Figure 5c). Subsequent irradiation with the green light regenerated the o-MOC-3 gel form. Stress-relaxation measurements enabled measurement of the relaxation times  $\tau$  of both o-gel and c-gel as 555 s and 1085 s, respectively. Since these values represented the thermally accelerated ligand exchange, they directly determined the self-healing behavior of the polyMOCs. The lower  $\tau$  value for o-MOC-3 (faster exchange) makes it more efficient in healing. The fatigue behavior of polyMOCs was also measured by means of the  $G'$  factor over several cycles of switching between two polymer topologies. The results obtained revealed an important relationship between polymer stability and length of radiation exposure. When the irradiation time was  $< 5 \text{ h}$ , the materials remained elastic for

seven cycles. However, prolonged exposure resulted in decay of the polyMOCs after only 4 cycles. This feature was attributed to the known photoinduced degradation of DTE under extended UV irradiation (Figure 5d).<sup>[139]</sup>

Previously, the same group studied a novel class of highly branched polyMOC gels with high functionality  $f$ .<sup>[140]</sup> To assess the impact of the  $f$  factor on polymer behavior, two different polyMOC gels were prepared. A low branch-functionality polymer based on an  $M_2L_4$  paddlewheel cluster (gel-2) and a compositionally isomeric  $M_{12}L_{24}$ -based polymer (gel-1) were obtained upon the reaction of  $Pd(NO_3)_2$  with bis-*meta*-pyridine-terminated PEG and bis-*para*-pyridine-terminated PEG in DMSO, respectively. In-depth studies showed the possibility of post-modification of gel-1 by replacing the defect with other free ligands, giving it new properties. The same protocol could not be applied to the low-branched gel-2.

Similarly, the use of a ligand functionalized star polymer, Pd metal salt, and non-functionalized ditopic ligand enabled three-component assembly leading to the formation of a star polyMOC gel.<sup>[141]</sup>

Beyond Pd-based polymers, Zhao et al. showed how subtle change in the number of hydroxyl groups can affect the overall behavior of polymeric elastomers.<sup>[142]</sup> They examined cages consisting of polytetramethylene glycol (PTMG) as polymeric soft domain and Rh-MOCs functionalized with different numbers of  $-OH$  groups acting as a crosslinkers. A higher number of hydroxyl moieties in elastic MOCs effectively increased both the storage modulus and tensile strength as well as the relaxation time.

A detailed study of cross-linked polymerization of Ru-MOCs has been made by Furukawa<sup>[143]</sup> involving in-depth studies on the mechanism of assembly of colloidal MOC gels,<sup>[144]</sup> the effects of chemical stimuli on the polymerization reaction,<sup>[145]</sup> ageing-induced structural transitions,<sup>[146]</sup> fabrication of soft materials through linker-exchange protocol<sup>[147]</sup> and the assembly of colloidal hydrogels from charged-MOCs.<sup>[148]</sup>

In a different approach, the group of Nitschke reported a polymeric hydrogel incorporating an imine-type MOC fitted with anionic subunits in the ligand backbone.<sup>[149]</sup> The reaction of 4,4-diaminobiphenyl-2,2-disulfonic acid with tetramethylammonium hydroxide and substituted pyridine aldehydes A–C in the presence of an iron(II) salt resulted in the formation of MOC-4a–c in aqueous solution (Figure 6a). The desired hydrogels gel-MOC-4b were obtained almost immediately when 15 wt% of the building blocks were used. In the case of the parent 2-formylpyridine A and short PEG-functionalized aldehyde C, polymerization did not occur, and only tetrahedral cages were formed, as established by  $^1H$  NMR spectroscopy. The concentration of the components affected the process of polymerization and when 10 wt% of substrates was used, formation of gel-MOC-4b required more time (5 min) and no hydrogel was formed with 5 wt%. Given the presence of cage cavities, subsequent study was made of guest binding and release. Fluorobenzene showed an affinity for the cage MOC-4a, with a binding constant  $K_a$  of  $6.1 \times 10^2 \text{ M}^{-1}$  and rate constant for guest uptake ( $k_{in}$ ) of  $2.21 \times 10^{-1} \text{ M}^{-1} \text{ s}^{-1}$ , as reported

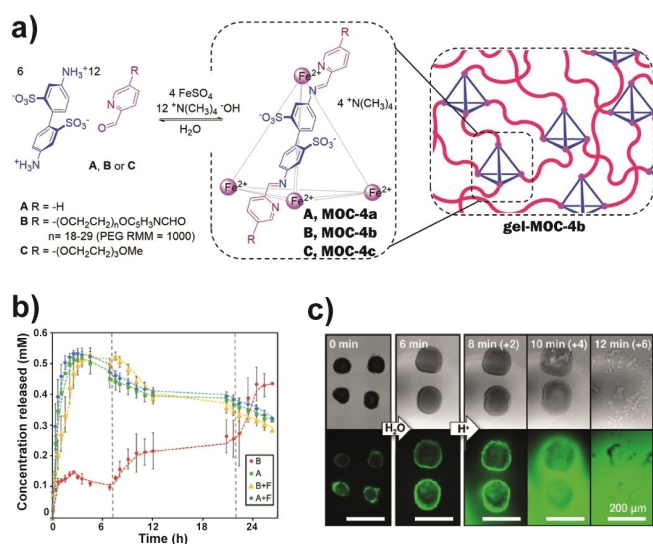


**Figure 6.** a) Synthesis of the **MOC-4** cages and hydrogel from 4,4-diaminobiphenyl-2,2-disulfonic acid, substituted pyridine aldehyde and iron sulfate; b) release profile of benzene (B) and anisole (A) in the presence or absence of furan (F); c) transmission microphotographs of hydrogel microparticles (top: optical, bottom: fluorescence) containing fluorescein isothiocyanate-dextran. Observable swelling upon hydration with water and disassembly after the addition of acid. Reproduced from Ref. [149] with permission. Copyright 2018, American Chemical Society.

previously.<sup>[150]</sup> In case of the 5 wt% cage **MOC-4b**, the addition of 8 equiv. of guest molecule resulted in the formation of a complex detected by a new resonance peak at  $-106.6$  ppm in the  $^{19}\text{F}$  NMR spectrum. When **gel-MOC-4b** was taken as a host molecule, initially no significant changes were observed but reexamination after a week showed encapsulation of guest, with the appearance again of a new  $^{19}\text{F}$  resonance. Further guest release studies with benzene, furan, and anisole were conducted in order to assess the binding mode—either through encapsulation inside the MOC cavity or in hydrogel pores. While the dilution of freshly prepared hydrogel previously equilibrated with an aqueous solution containing 1:1 mixture of benzene and anisole caused the release of the anisole from the gel to supernatant within 3 h, reaching its concentration of  $0.54$  mM, only a slight increase in the concentration of benzene in solution ( $0.14$  mM) was observed. However, the subsequent addition of furan solution after 7 h resulted in a significant release of benzene from cage, as the concentration in the solution increased to  $0.26$  mM after 22 h and  $0.43$  mM after 26 h. No corresponding increase in the concentration of anisole was observed, as shown in Figure 6b. Very similar results were obtained when an aqueous solution of furan was added at the beginning of experiments, leading to increases in the concentration of both benzene and anisole up to  $0.52$  mM and  $0.53$  mM, respectively. These experiments clearly confirmed the different nature of guest binding, with anisole occupying the pores of hydrogel pores and benzene mostly encapsulating the cavity of cage. In order to measure the retention and release of hydrogel cargoes, microparticles loaded with fluorescein isothiocya-

nate-dextran were made using a three-input microfluidic device. With this guest, cargo diffusion was readily monitored by fluorescence microscopy. It was shown thereby that although the hydration of microparticles affects the swelling of the material, there was no significant loss of cargo. Acidification of the sample resulted in microparticle disassembly through the decomposition of cage and thus complete release of the cargo to the surrounding medium (Figure 6c).

A quite different approach for the formation of 1DM is that of Kumar et al., using a strategy for stabilizing MOCs on single-walled carbon nanotubes (SWNT).<sup>[151]</sup> A cage based on the common paddlewheel  $\text{Cu}_2$  unit and 5-hydroxyisophthalate organic ligand was prepared. The surface of the SWNTs was modified by treatment with a  $\text{HNO}_3/\text{H}_2\text{SO}_4$  mixture in order to form carboxylic acid groups on the surface. Subsequent reaction of both components (cage and SWNT) in methanol resulted in the formation of a nanocomposite with MOC to NT weight ratio of 1:2 or 1:1. The 1DM was considered to be stabilized through ester bond formation between the hydroxyl moiety of the cage and the carboxylic acid of the NT as well as  $\pi$ - $\pi$  and ion-covalent interactions between Cu of MOC and carboxylates of SWNT. It exhibits a BET surface area of  $\approx 300$   $\text{m}^2$   $\text{g}^{-1}$  as well as good catalytic properties in the heterogeneous conversion of epoxides to cyclic carbonates. In comparison to the pristine MOC, the yield of the catalytic reaction was 67% higher when MOC@NT was used.

The various examples of 1DM structures decorated with MOCs and OCs cages serve as an indicator of the growing demand for such systems. As technological advancements continue, newer and more efficient systems are necessary, particularly in processes that involve filtration, purification, or recovery of raw materials. The construction of polymers that possess dynamic architectures, or even their complete synthesis, appears to be fulfilling its purpose, given the successful separation processes (among other things) carried out on the aforementioned systems. Eliminating any remaining issues, such as uneven cage deposition or limited stability of dynamic systems, will undoubtedly enhance the properties of these already highly advanced smart materials.

### 3.3. 2D Materials

Ultrathin two-dimensional materials (2DMs) are a new class of nanomaterials with sheet-like structures and lateral dimensions ranging from hundreds of nanometers to several microns, while their thickness is typically less than  $5$  nm.<sup>[152]</sup> Due to their unique shapes, 2D nanomaterials possess a very large surface and have anisotropic physical/chemical properties.<sup>[152]</sup> Depending on the type of surface, 2DMs have found emerging applications in electronics (sensing, spintronics), optoelectronics (photovoltaics, emitters), and energy (batteries, supercapacitors).<sup>[153]</sup> Modifications of the surfaces with self-assembled structures are expected to lead to the development of molecular devices with specific functions such as sensing of various analytes or improved catalytic properties of the composites.

Several examples of engineering of 2DMs with dynamic supramolecular cages have been reported as a way to generate surface-assisted molecular containers. Such functionalization can be done by self-assembly processes with the aid of non-covalent intermolecular interactions (e.g., electrostatics),<sup>[154]</sup> as well as by the formation of covalent bonds between the cage and self-assembled monolayers (SAMs) of the pre-functionalized 2DMs.<sup>[86]</sup>

Effective hybridization of MOCs with a silicon surface has been reported by the group of Dalcanale.<sup>[155]</sup> Formation of such inorganic-organic material required a two-step approach: 1) grafting of a designed cavitand onto a Si–H surface through hydrosilylation reaction; 2) formation of desired MOCs through ligand exchange between the surface bounded cavitand and preformed, highly soluble bis-(cavitand)Pt cage. In this regard, a tolylpyridine resorcinarene with terminally functionalized 1-octene chains was used to obtain the Si-immobilized monolayer. The pyrene functionalized “capping” pyridine-based cavitand has been designed to enable the characterization of grafted heterocage with spectroscopic methods. Additionally, a prospect of single molecule sensing was suggested for this material.

Significant progress in the functionalized 2DM area has been made with the use of gold surfaces. Straightforward thiol-functionalization of a gold SAM has allowed for the incorporation of different types of dynamic cages. Garcia-Lopez<sup>[156]</sup> has described functionalization of an Au SAM with hydrogen-bonded cages. Successful fabrication of a coated gold surface was achieved through an exchange reaction between calix-[4]arene dimelamine attached to hexanethiol-Au monolayers and a previously synthesized hydrogen-bonded cage. Although this composite material has not been investigated in terms of possible applications, it constitutes the only example of a fabricated 2D SAM with finite nanometer sized hydrogen-bonded assemblies.

The assembly of MOCs on gold monolayers was also investigated by the group of Reinhoudt. In 2001, a protocol for monitoring MOCs formation on sulfanylundecanol-functionalized Au monolayers utilizing atomic force microscopy (AFM) was described.<sup>[157]</sup> A cavitand possessing two oppositely located functional groups, sulfide-alkyl chains, and nitrile moieties, allowed at first the formation of functionalized SAM, and subsequent cages assembly via metal-induced coordination in presence of an appropriate Pd<sup>2+</sup> or Pt<sup>2+</sup> metal salts. AFM analysis of the fabricated Au-SAM revealed dots with different heights attributed to either cavitand or cages adsorbed on the surface. Further studies enabled the formation of heterocage attached to the 2D gold monolayer.<sup>[158]</sup> While the general protocol for the formation of fabricated SAMs remained the same as in previous work, in this study a resorcinarene-based cavitand containing tolylpyridine groups at the upper rim was used as the ligand for the coordination with Pd<sup>2+</sup>/Pt<sup>2+</sup> salts. The lower rim of the scaffold incorporated alkylthioether chains, suitable for adsorption on Au. In order to obtain a self-assembled heterocage, the cavitand-decorated SAM was exposed to the solution of cage composed of cavitands, differing in substituent at the lower rim of the resorcinarene

skeleton. Successful ligand exchange was confirmed through AFM imaging.

Another interesting example from the same group demonstrated the effect of multiple hydrophobic interactions between a bis(adamantyl)-functionalized calix[4]arene and EDTA-tethered  $\beta$ -cyclodextrin (CD) dimer on cage formation both in solution and adsorbed on the self-assembled gold monolayer.<sup>[159]</sup> It was shown that the binding constant between the substrate in solution was three orders of magnitude weaker than in the cage formed on the Au surface.

As shown by Yuan et al. the Au(111) 2D surface can also be suitable for attachment of dynamic coordination architectures, including rectangular and square macrocycles as well as three-dimensional cages.<sup>[160]</sup> The scanning tunneling microscopy (STM) imaging of the solid materials revealed ordered adlayers, specific for each of the adsorbed molecules. However, upon self-organization of a binary system solution on the Au surface, an easily distinguishable two-phase surface was detected, without an additional mixed adlayer.

Kumar et al. has reported a new strategy for the stabilization of MOCs on graphene, leading to the formation of new 2D composite material with significantly enhanced catalytic activity compared to the pristine cage, similar to the previously described **MOC-5/NT**.<sup>[151]</sup> Thus, **MOC-5** was used in functionalization of a 2D carboxylated-graphene basal plane (Figure 7a,b). Newly obtained composites **MOC-5/Gr-1,2,3** differed in cage to graphene weight ratios of 1:4, 1:2 and 1:1, respectively. While the pristine cage exhibited low N<sub>2</sub> uptake due to its agglomeration restricting it to small pore volumes (0.1 cm<sup>3</sup> g<sup>-1</sup>), good dispersion of the MOC on graphene surfaces provided higher pore volumes in the range of 0.9–1 cm<sup>3</sup> g<sup>-1</sup>. The presence of Lewis acid sites (Cu<sub>2</sub> units) increased the activity of composites as heterogeneous catalysts. Conversion of propylene oxide into propylene carbonate was chosen as test reaction and with the 0.03 mol% loading of catalyst **MOC-5/GR-2** and nBu<sub>4</sub>NBr as co-catalyst, 80 % enhancement in catalytic activity was observed, with an oxide conversion of 56 %, in comparison to MOC-catalyzed reaction (31 % yield conversion).

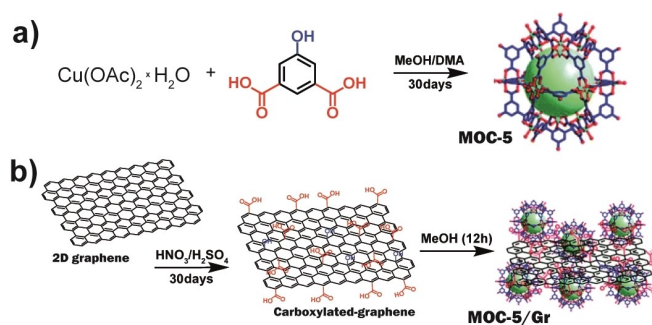


**Figure 7.** a) Synthesis of hydroxylated **MOC-5** from its components; b) functionalization of a graphene layer with carboxylic moieties followed by the formation of the **MOC-5/Gr** nanocomposite. Reproduced from Ref. [151] with permission. Copyright 2017, Royal Society of Chemistry.

Despite the wide structural versatility of MOCs and OCs the process of embedding these architectures on 2D surfaces remains a very challenging task mainly due to the possibility of under-controlled material deposition. Nevertheless, the examples presented in the above section confirm the validity of continuing work on the efficient and controlled creation of new composites based on cage-functionalized 2DMs as they present high application potential, e.g., in heterogeneous catalysis. 2DMs play a large part in a number of high-profile fields, e.g., flexible electronics and the ability to integrate a cage-based receptors on the surface that controls the specificity of the 2DM is certainly worthwhile pursuit.

### 3.4. 3D Systems

Among the different nanostructures that have been demonstrated as promising materials for various applications, 3D nanostructures have attracted significant attention as building blocks for constructing high-performance nanodevices.<sup>[161]</sup> It is not surprising then that programming three-dimensional nanostructures into functional materials is becoming increasingly important given the need for ever more highly functional solids. The most common 3D solids exhibiting practical properties and being useable in real life are MOFs.<sup>[2]</sup> These metal coordination-based porous frameworks, due to their high surface areas and functional pores, have a bright potential for application in separation, storage,<sup>[162]</sup> and sensing<sup>[163]</sup> processes but also in catalysis,<sup>[164]</sup> biomedicine<sup>[165]</sup> and even as electric and magnetic materials.<sup>[166,167]</sup>

A new trend, aimed at increasing the application potential of such systems, involves incorporation of additional substances with their own internal void (cages) into the MOF structure. Such modification is beneficial to both compounds. On the one hand, the incorporated cage is shielded from the action of external chemical factors (temperature, type of solvent) that could cause its disintegration. On the other, encapsulated cages improve the properties of the framework, influencing its functionality. Thus, the integration of MOFs and MOCs architectures into the 3D systems paves the way for precisely designed materials with unique structural features and resulting better conductivity than pristine building blocks. Deng et al. performed for the first time the successful synthesis of a 3D material by incorporating both organic (enzyme) or inorganic (MOC) molecules into the interior of crystalline IRMOF-74-IV, through the immersion of the activated MOF into the solution containing the desired cage-guest.<sup>[168]</sup> Although study of the physicochemical properties of this system was not the principal objective of the work, it represents a milestone in the development of functional MOF@MOC systems. Since then, several research groups have successfully developed new methods for the inclusion of MOCs into the voids of crystalline MOF networks, influencing their application potential. In this regard, Luo et al. performed the heterogenization of a photochemically active metal-organic cage (MOC-6) into a Zn-based MOF in order to obtain a highly efficient molecular device for

proton and electron transfer (Figure 8a).<sup>[169]</sup> While the bimetallic cage  $[\text{Pd}_6(\text{RuL}_3)_8]^{28+}$  ( $\text{L} = 2\text{-}(\text{pyridin-3-yl})\text{-1H-imidazo}[4,5-f][1,10]\text{-phenanthroline}$ ) has already been described as good photochemical molecular device (PMD) with well-organized multiple photosensitizers and catalyzers for efficient  $\text{H}_2$  generation,<sup>[170,171]</sup> it continues to suffer from limited stability after long irradiation times. To prevent unfavorable degradation, MOC-6 was incorporated inside the cavity of the MOF (ZIF-8) via a coordination-assisted secondary assembly process. Given the larger size of the cage compared to the pore dimensions, the MOC@MOF composite was obtained by superimposing the MOF components onto the already formed cage. In the final stage, structural transformation in the presence of  $\text{CO}_2$  and  $\text{H}_2\text{O}$  allowed the formation of the desired carbonized MOC-6@CZIF-8—a solid that is both resistant to ambient conditions and retains effective photophysical and photochemical features. Comparison of the photocatalytic properties of pristine MOC-6 and MOC-6@CZIF-8, fully confirmed the utility of the modification of metal-organic networks, based on the  $\text{H}_2$  generation process. Evolution curves obtained for the MOC-6@CZIF-8 in the presence of the necessary sacrificial agent 1,3-dimethyl-2-phenyl-2,3-dihydro-1H-benzimidazole (BIH), showed  $32.4 \text{ mmol} \cdot \text{g}^{-1} \text{ H}_2$  output after 8 h of the first cycle, whether in  $\text{N}_2$  or  $\text{CO}_2$  atmospheres. Interestingly non-carbonized MOC@MOF

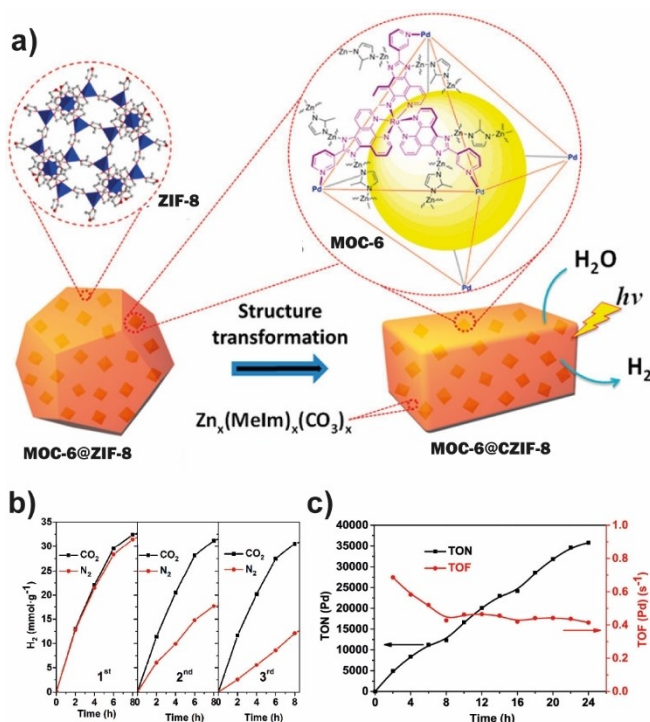


**Figure 8.** a) Schematic formation of the MOC-6/CZIF-8 matrix through the incorporation of MOC-6 into a ZIF-8 MOF followed by carbonization of the composite; b)  $\text{H}_2$  evolution curves for MOC-6/CZIF-8 in an  $\text{N}_2$  and  $\text{CO}_2$  atmosphere for three consecutive cycles; c) accumulated TOF and TON of the catalyst durability test over 24 h. Reproduced from Ref. [169] with permission. Copyright 2019, American Chemical Society.

showed nearly zero catalytic activity in an  $N_2$  atmosphere but was comparable to the carbonized analogue for the process under  $CO_2$  conditions ( $\approx 31.9 \text{ mmol} \cdot \text{g}^{-1}$ ). This is due to the sensitivity of the **ZIF-8** to  $CO_2$  resulting in the simultaneous conversion of the material to a highly active **MOC@CMOF** matrix. In testing the catalytic activity, several cycles of the  $H_2$  generation were investigated. The overall turnover number (TON) and the momentary turnover frequency (TOF) for **MOC-6@CZIF-8** after 8 hours of the photocatalytic process in a  $CO_2$  atmosphere were  $\sim 12317$  and  $0.43 \text{ H}_2\text{s}^{-1}$ , respectively, based on the number Pd centers. The values obtained are significantly higher than those of a homogeneous MOC ( $635$  and  $30 \text{ H}_2\text{h}^{-1}$ , respectively in 48 h), as shown in Figure 8b,c). In contrast, carbonization of the ZIF-matrix appears to have no effect on electrical conductivity, since both composites exhibit similar conductivity of  $\sim 10^{-10} \text{ Scm}^{-1}$ . Hardly different results were obtained for samples in which the sacrificial agent was applied onto the catalyst. A significant increase of the conductivity of  $\sim 10^{-9} \text{ Scm}^{-1}$  was attributed to the presence of redox-active guest molecules.<sup>[172,173]</sup>

Taking advantage of the large pore size of a robust mesoporous **PCN-777** MOF, Lee et al. described the synthesis of a MOC@MOF composite using a wet impregnation method.<sup>[174]</sup> By dissolving a Cu-based paddlewheel cuboctahedron metal-organic cage possessing 5-sulfoisophthalic acid moieties as a bridging ligand, in a small amount of methanol and mixing it with the insoluble MOF, two distinct materials have been generated, which differ in the number of incorporated MOCs in a unit cell of **PCN-777**, 2,7 and 3,7 cages encapsulated respectively. Interestingly, the PXRD pattern of the obtained materials was the same as the pristine MOF, confirming the intact crystallinity of MOF after wet impregnation. Despite this, their properties differed from the non-functionalized MOF, showing not only increased polarity compared to pure **PCN-777** and the resulting 1.5-fold higher water vapor adsorption capacities but also enhanced proton conductivity from  $5.69 \times 10^{-8}$  to  $2.11 \times 10^{-4} \text{ Scm}^{-1}$ .

While the wet impregnation approach can be suitable for smaller size guest molecules that can easily fit into the MOF's pores, a different approach for the inclusion of larger MOCs has to be utilized. One of the methods described by the group of Zhang is two-step post-assembly incorporation, suitable for the formation of Zr-MOC at **DUT-68**.<sup>[175]</sup> At first, an organic ligand was introduced into the cavity of hydrolytically stable MOF by stirring them together under aqueous conditions for 24 h, followed by gradual addition of an aqueous solution of Zr salt. The material obtained exhibited a proton conductivity of  $1.14 \times 10^{-3} \text{ Scm}^{-1}$  at 98 % relative humidity (RH) and  $80^\circ\text{C}$ . Interestingly, this value is about two orders of magnitude greater than that of the pristine MOF ( $8.83 \times 10^{-6} \text{ Scm}^{-1}$ ), as well as roughly 110 % higher than that of a composite obtained by wet impregnation ( $1.03 \times 10^{-4} \text{ Scm}^{-1}$ ).

Similarly, Qui et al. have reported an efficient hydrophilicity-directed approach (HDA) for the encapsulation of MOCs composed of 1,3,5-tris(4-pyridyl)-2,4,6-triazine and (en)Pd(NO<sub>3</sub>)<sub>2</sub>. This method is designed for MOCs larger,

than the MOF's aperture size.<sup>[176]</sup> In contrast to the methods described previously in this paragraph, the driving force behind the formation of the described 3D MOC@MOF composite is the change in the polarity of the reaction medium. Due to the hydrophilic nature of the inner surface of designed MOF, the addition of an aqueous solution of metal salt to a mixture of the ligand and MOF (**MIL-101**) in hexane shifted the chemical equilibrium of the reaction toward self-assembly of the water-soluble cage inside the MOF's pores. The PXRD patterns of MOC@MOF-*N* composite (where *N* stands for the average number of cages accommodated in the **MIL-101** cavities) were identical to those of the pristine MOF, affirming the intact structure of the framework. The successful incorporation of the cage was confirmed with <sup>13</sup>C solid-state NMR as well as Fourier Transform infrared spectroscopy (FTIR). Further research revealed a high application potential of the obtained composites in the selective oxidation of benzyl alcohol. The yield of the reaction carried out by means of obtained 3D system was 20 times higher than that of MOC itself, even after 5 cycles of the process.

Depending on the type of MOF pore size, successful incorporation of MOCs into its cavity, can be carried out using several approaches (wet impregnation, HDA, coordination-assisted secondary assembly process). Regardless of the synthetic route, the obtained 3D composites are characterized by much better physicochemical properties such as storage capacity, photocatalytic activity, or electrical conductivity, compared to their individual components. In some cases, a stabilization effect of the cages can also be observed, protecting them from the adverse effects of the reaction medium. The proposed examples perfectly demonstrate the advantages of creating composite materials, and most likely further development of this field of chemistry will contribute to the synthesis of even more sophisticated and efficient systems with desirable functions.

#### 4. Summary and Outlook

This Review attempts to expand the scope of multidimensional, cage-functionalized smart materials and summarize the strategies behind their efficient syntheses affecting application potential. Not surprisingly, dynamic cages have found their use in the fabrication of a variety of solid materials to serve as a foundational element for newly created 0–3 dimensional architectures. Both MOCs and OCs have been a subject of great interest to chemists from all over the world for several decades, which translates into a wealth of knowledge related to synthesis, functionalization, post-modification, and, finally, their practical application. With the development of metallosupramolecular chemistry as well as dynamic covalent chemistry, scientists have begun to equip the newly created cage architectures with a variety of properties, such as photoactive or luminescent features, chiral attributes, or the ability to recognize various guest molecules (including biological active substances, hazardous/toxic/explosive molecules, greenhouse gases or elements of environmental pollution). The latter significantly increased

the interest and potential use of cages in biological systems. However, in parallel with the numerous advantages of cage-like architectures, they also go hand in hand with some drawbacks. The reversibility of connections, which is a key element in template synthesis, thermodynamic equilibrium of formation processes, or specific response to stimuli is often a limiting factor in the use of the cages. Vulnerability to environmental changes largely limits the use of dynamic cages more widely than it has been recognized. Despite attempts to offset the negative effects of several factors on the stability of reversible bonds, the synthesis of the aforementioned architectures often requires a strict balance between the dynamicity and stability of the target systems.

And when it might seem that the topic of reversible molecular and supramolecular systems is proverbially “exhausted,” the combination of the already well-known chemistry in solution (but not only) with a separate branch of chemistry—materials chemistry, has contributed to the renewed flourishing of dynamic cages. This time as part of smart materials with different dimensionality, sensitivity towards external factors, and sometimes even different properties than the pristine cage.

The development of surface-active materials has been a true breakthrough in materials science. So far, enormous progress has already been achieved in the field of modified surfaces, leading to the fabrication of functionalized systems varying in types of molecules attached to the chosen material, thus exploiting diverse properties, from conductivity, through catalysis to separation processes. One such modification, affecting the specific features of a given material, is the introduction of molecular or supramolecular cage-like architectures, mainly based on covalent or coordination bonds. The use of different types of substrates (0D NPs, 1D systems, 2D surfaces, or 3D MOFs) fabricated with caged systems represents a step forward in the creation of smart materials whose properties are either superior to those of the building blocks (composites) or even fundamentally different (hybrids). This combination is advantageous for several reasons. The introduction of dynamic features into previously characterized solid materials provides them with properties that can be tuned with external stimuli (e.g., UV light, solvent, temperature) inducing a micro- or macroscopic structural change, increasing their potential application. The combination with the substrate also brings positive aspects to the cages themselves. Not only cage stability is increased by eradicating the negative effects of the reaction medium, but also the efficiency of the processes in which they participate is significantly improved.

Although enormous progress made in the formation of nanostructured smart materials with promising features has been summarized in this Review, this field is still in its infancy, and some of the challenges and limitations still require deep scientific attention. For example, increased structural diversity is needed to expand the library of potential functions, but also new strategies for defect-free molecular packing onto/into substrates increasing the efficiency of the formation of these materials as well as the very processes they participate in. This applies to a wide range of applications, including molecular recognition. For now, the

examination of this principle by highly complex systems is far from trivial. It is expected that as the field of smart materials continues to grow and new analytical methods capable of addressing this challenging task will be developed. A key step will also be the translation of research results into a practical application of materials in major industrial processes related to the environment (filtration, separation, purification) or the broad energy sector (conductivity, energy transfer). Thus, there is still a room for the development of this field of chemistry. So long as the quality of the broad arsenal of 0D to 3D smart material continues to improve, more breakthroughs can be expected in the field of functional systems.

One general purpose of this Review was to inspire scientists to develop strategies that can be used for the formation of new functional smart materials with precisely defined properties. The findings discussed above are a selection intended to illustrate significant developments in the field of materials science. An attempt has been made to show the promise of dynamic chemistry in the context of functionalization of multidimensional (from 0D to 3D) active surfaces and to summarize the strategies required for their effective decoration with cage-like architectures.

### Acknowledgements

The work was supported by the National Science Centre of Poland (grants SONATA BIS 2018/30/E/ST5/00032 (ARS), SONATINA UMO-2019/32/C/ST4/00565 (WD)).

### Conflict of Interest

The authors declare no conflict of interest.

### Data Availability Statement

Data sharing is not applicable to this article as no new data were created or analyzed in this study.

**Keywords:** Dynamic Cages · MOCs · Nanocomposites · Smart Materials · Surface Functionalization

- [1] X.-Y. Yang, L.-H. Chen, Y. Li, J. C. Rooke, C. Sanchez, B.-L. Su, *Chem. Soc. Rev.* **2017**, *46*, 481–558.
- [2] B. S. Pilgrim, N. R. Champness, *ChemPlusChem* **2020**, *85*, 1842–1856.
- [3] J. J. Perry Iv, J. A. Perman, M. J. Zaworotko, *Chem. Soc. Rev.* **2009**, *38*, 1400–1417.
- [4] Y. Xue, S. Zheng, H. Xue, H. Pang, *J. Mater. Chem. A* **2019**, *7*, 7301–7327.
- [5] D. J. Tranchemontagne, Z. Ni, M. O’Keeffe, O. M. Yaghi, *Angew. Chem. Int. Ed.* **2008**, *47*, 5136–5147.
- [6] E. Sánchez-González, M. Y. Tsang, J. Troyano, G. A. Craig, S. Furukawa, *Chem. Soc. Rev.* **2022**, *51*, 4876–4889.
- [7] A. J. McConnell, *Chem. Soc. Rev.* **2022**, *51*, 2957–2971.
- [8] J. E. M. Lewis, *Chem. Commun.* **2022**, *58*, 13873–13886.

- [9] D. A. Roberts, B. S. Pilgrim, J. R. Nitschke, *Chem. Soc. Rev.* **2018**, *47*, 626–644.
- [10] N. Ahmad, H. A. Younus, A. H. Chughtai, F. Verpoort, *Chem. Soc. Rev.* **2015**, *44*, 9–25.
- [11] Y. Xue, X. Hang, J. Ding, B. Li, R. Zhu, H. Pang, Q. Xu, *Coord. Chem. Rev.* **2021**, *430*, 213656.
- [12] A. Galan, P. Ballester, *Chem. Soc. Rev.* **2016**, *45*, 1720–1737.
- [13] M. Han, D. M. Engelhard, G. H. Clever, *Chem. Soc. Rev.* **2014**, *43*, 1848–1860.
- [14] C. J. Pugh, V. Santolini, R. L. Greenaway, M. A. Little, M. E. Briggs, K. E. Jelfs, A. I. Cooper, *Cryst. Growth Des.* **2018**, *18*, 2759–2764.
- [15] A. R. Hughes, N. J. Brownbill, R. C. Lalek, M. E. Briggs, A. G. Slater, A. I. Cooper, F. Blanc, *Chem. Eur. J.* **2017**, *23*, 17217–17221.
- [16] S. Xu, P. Li, Z.-Y. Li, C. Yu, X. Liu, Z. Liu, S. Zhang, *CCS Chem.* **2021**, *3*, 1838–1850.
- [17] Q. Wang, C. Yu, C. Zhang, H. Long, S. Azarnoush, Y. Jin, W. Zhang, *Chem. Sci.* **2016**, *7*, 3370–3376.
- [18] C. Givélet, J. Sun, D. Xu, T. J. Emge, A. Dhokte, R. Warmuth, *Chem. Commun.* **2011**, *47*, 4511–4513.
- [19] X. Liu, R. Warmuth, *J. Am. Chem. Soc.* **2006**, *128*, 14120–14127.
- [20] T. Hasell, X. Wu, J. T. A. Jones, J. Bacsá, A. Steiner, T. Mitra, A. Trewin, D. J. Adams, A. I. Cooper, *Nat. Chem.* **2010**, *2*, 750–755.
- [21] X. Yang, Z. Ullah, J. F. Stoddart, C. T. Yavuz, *Chem. Rev.* **2023**, *123*, 4602–4634.
- [22] T. Hasell, A. I. Cooper, *Nat. Rev. Mater.* **2016**, *1*, 16053.
- [23] H. Wang, Y. Jin, N. Sun, W. Zhang, J. Jiang, *Chem. Soc. Rev.* **2021**, *50*, 8874–8886.
- [24] W. Cao, J. Zhou, Z. Kochovski, H. Miao, Z. Gao, J.-K. Sun, J. Yuan, *Cell Rep. Phys. Sci.* **2021**, *2*, 100546.
- [25] M. W. Schneider, I. M. Oppel, A. Griffin, M. Mastalerz, *Angew. Chem. Int. Ed.* **2013**, *52*, 3611–3615.
- [26] J. Liu, Z. Wang, P. Cheng, M. J. Zaworotko, Y. Chen, Z. Zhang, *Nat. Chem. Rev.* **2022**, *6*, 339–356.
- [27] E.-S. M. El-Sayed, D. Yuan, *Chem. Lett.* **2020**, *49*, 28–53.
- [28] E. Raee, Y. Yang, T. Liu, *Giant* **2021**, *5*, 100050.
- [29] H. Amouri, C. Desmaretz, J. Moussa, *Chem. Rev.* **2012**, *112*, 2015–2041.
- [30] T. R. Cook, P. J. Stang, *Chem. Rev.* **2015**, *115*, 7001–7045.
- [31] S. Zarra, D. M. Wood, D. A. Roberts, J. R. Nitschke, *Chem. Soc. Rev.* **2015**, *44*, 419–432.
- [32] E. G. Percástegui, T. K. Ronson, J. R. Nitschke, *Chem. Rev.* **2020**, *120*, 13480–13544.
- [33] D. Zhang, T. K. Ronson, Y.-Q. Zou, J. R. Nitschke, *Nat. Chem. Rev.* **2021**, *5*, 168–182.
- [34] D. Philp, J. F. Stoddart, *Angew. Chem. Int. Ed. Engl.* **1996**, *35*, 1154–1196.
- [35] Y. Lu, D. Liu, Y.-J. Lin, Z.-H. Li, G.-X. Jin, *Natl. Sci. Rev.* **2020**, *7*, 1548–1556.
- [36] X. Han, G. Liu, S. H. Liu, J. Yin, *Org. Biomol. Chem.* **2016**, *14*, 10331–10351.
- [37] Y. Domoto, M. Fujita, *Coord. Chem. Rev.* **2022**, *466*, 214605.
- [38] J. Singh, H. Kim, K.-W. Chi, *Chem. Rec.* **2021**, *21*, 574–593.
- [39] S. Lee, A. Yang, T. P. Money Penny, II, J. S. Moore, *J. Am. Chem. Soc.* **2016**, *138*, 2182–2185.
- [40] Q. Wang, C. Yu, H. Long, Y. Du, Y. Jin, W. Zhang, *Angew. Chem. Int. Ed.* **2015**, *54*, 7550–7554.
- [41] K. E. Jelfs, X. Wu, M. Schmidtman, J. T. A. Jones, J. E. Warren, D. J. Adams, A. I. Cooper, *Angew. Chem. Int. Ed.* **2011**, *50*, 10653–10656.
- [42] S. Hong, M. R. Rohman, J. Jia, Y. Kim, D. Moon, Y. Kim, Y. H. Ko, E. Lee, K. Kim, *Angew. Chem. Int. Ed.* **2015**, *54*, 13241–13244.
- [43] T. Tozawa, J. T. A. Jones, S. I. Swamy, S. Jiang, D. J. Adams, S. Shakespeare, R. Clowes, D. Bradshaw, T. Hasell, S. Y. Chong, C. Tang, S. Thompson, J. Parker, A. Trewin, J. Bacsá, A. M. Z. Slawin, A. Steiner, A. I. Cooper, *Nat. Mater.* **2009**, *8*, 973–978.
- [44] T. Hasell, J. L. Culshaw, S. Y. Chong, M. Schmidtman, M. A. Little, K. E. Jelfs, E. O. Pyzer-Knapp, H. Shepherd, D. J. Adams, G. M. Day, A. I. Cooper, *J. Am. Chem. Soc.* **2014**, *136*, 1438–1448.
- [45] M. Kołodziejski, A. R. Stefankiewicz, J.-M. Lehn, *Chem. Sci.* **2019**, *10*, 1836–1843.
- [46] R. Modak, B. Mondal, P. Howlader, P. S. Mukherjee, *Chem. Commun.* **2019**, *55*, 6711–6714.
- [47] K. Acharyya, P. S. Mukherjee, *Chem. Commun.* **2014**, *50*, 15788–15791.
- [48] W. Drożdż, C. Bouillon, C. Kotras, S. Richeter, M. Barboiu, S. Clément, A. R. Stefankiewicz, S. Ulrich, *Chem. Eur. J.* **2017**, *23*, 18010–18018.
- [49] A. R. Stefankiewicz, M. R. Sambrook, J. K. M. Sanders, *Chem. Sci.* **2012**, *3*, 2326–2329.
- [50] K. R. West, K. D. Bake, S. Otto, *Org. Lett.* **2005**, *7*, 2615–2618.
- [51] M. Konopka, P. Cecot, J. M. Harrowfield, A. R. Stefankiewicz, *J. Mater. Chem. C* **2021**, *9*, 7607–7614.
- [52] S. P. Black, J. K. M. Sanders, A. R. Stefankiewicz, *Chem. Soc. Rev.* **2014**, *43*, 1861–1872.
- [53] G. Zhang, O. Presly, F. White, I. M. Oppel, M. Mastalerz, *Angew. Chem. Int. Ed.* **2014**, *53*, 1516–1520.
- [54] S. Klotzbach, F. Beuerle, *Angew. Chem. Int. Ed.* **2015**, *54*, 10356–10360.
- [55] K. E. Jelfs, A. I. Cooper, *Curr. Opin. Solid State Mater. Sci.* **2013**, *17*, 19–30.
- [56] E. Berardo, L. Turcáni, M. Miklitz, K. E. Jelfs, *Chem. Sci.* **2018**, *9*, 8513–8527.
- [57] E. Berardo, R. L. Greenaway, M. Miklitz, A. I. Cooper, K. E. Jelfs, *Mol. Syst. Des. Eng.* **2020**, *5*, 186–196.
- [58] A. Tarzia, K. E. Jelfs, *Chem. Commun.* **2022**, *58*, 3717–3730.
- [59] M. A. Little, A. I. Cooper, *Adv. Funct. Mater.* **2020**, *30*, 1909842.
- [60] J. T. A. Jones, D. Holden, T. Mitra, T. Hasell, D. J. Adams, K. E. Jelfs, A. Trewin, D. J. Willock, G. M. Day, J. Bacsá, A. Steiner, A. I. Cooper, *Angew. Chem. Int. Ed.* **2011**, *50*, 749–753.
- [61] T. Mitra, K. E. Jelfs, M. Schmidtman, A. Ahmed, S. Y. Chong, D. J. Adams, A. I. Cooper, *Nat. Chem.* **2013**, *5*, 276–281.
- [62] N. Ahmad, A. H. Chughtai, H. A. Younus, F. Verpoort, *Coord. Chem. Rev.* **2014**, *280*, 1–27.
- [63] T. Tateishi, M. Yoshimura, S. Tokuda, F. Matsuda, D. Fujita, S. Furukawa, *Coord. Chem. Rev.* **2022**, *467*, 214612.
- [64] Z. Meng, F. Yang, X. Wang, W.-L. Shan, D. Liu, L. Zhang, G. Yuan, *Inorg. Chem.* **2023**, *62*, 1297–1305.
- [65] A. Brzechwa-Chodzyńska, W. Drożdż, J. Harrowfield, A. R. Stefankiewicz, *Coord. Chem. Rev.* **2021**, *434*, 213820.
- [66] F. J. Rizzuto, L. K. S. von Krbek, J. R. Nitschke, *Nat. Chem. Rev.* **2019**, *3*, 204–222.
- [67] C. T. McTernan, J. A. Davies, J. R. Nitschke, *Chem. Rev.* **2022**, *122*, 10393–10437.
- [68] S. Chen, L.-J. Chen, *Chemistry* **2022**, *4*, 494–519.
- [69] L. An, P. De La Torre, P. T. Smith, M. R. Narouz, C. J. Chang, *Angew. Chem. Int. Ed.* **2023**, *62*, e202209396.
- [70] Z. S. Qian, X. Y. Shan, L. J. Chai, J. R. Chen, H. Feng, *Biosens. Bioelectron.* **2015**, *68*, 225–231.
- [71] S. Lu, G. Li, Z. Lv, N. Qiu, W. Kong, P. Gong, G. Chen, L. Xia, X. Guo, J. You, Y. Wu, *Biosens. Bioelectron.* **2016**, *85*, 358–362.

- [72] X. Yan, Y. Song, C. Zhu, J. Song, D. Du, X. Su, Y. Lin, *ACS Appl. Mater. Interfaces* **2016**, *8*, 21990–21996.
- [73] S. Pandit, P. Behera, J. Sahoo, M. De, *ACS Appl. Bio Mater.* **2019**, *2*, 3393–3403.
- [74] C. Zhang, J. He, Y. Zhang, J. Chen, Y. Zhao, Y. Niu, C. Yu, *Biosens. Bioelectron.* **2018**, *102*, 94–100.
- [75] A. Barberis, Y. Spissu, A. Fadda, E. Azara, G. Bazzu, S. Marceddu, A. Angioni, D. Sanna, M. Schirra, P. A. Serra, *Biosens. Bioelectron.* **2015**, *67*, 214–223.
- [76] N. Bagheri, A. Khataee, B. Habibi, J. Hassanzadeh, *Talanta* **2018**, *179*, 710–718.
- [77] U. Jain, N. Chauhan, *Biosens. Bioelectron.* **2017**, *89*, 578–584.
- [78] J. Ou, H. Tan, Z. Chen, X. Chen, *Sensors* **2019**, *19*, 1455.
- [79] H. Zhang, X. Dong, J. Wang, R. Guan, D. Cao, Q. Chen, *ACS Appl. Mater. Interfaces* **2019**, *11*, 32489–32499.
- [80] Z. Wang, T. Hu, R. Liang, M. Wei, *Front. Chem.* **2020**, *8*, 320.
- [81] L. Wang, L. Xu, H. Kuang, C. Xu, N. A. Kotov, *Acc. Chem. Res.* **2012**, *45*, 1916–1926.
- [82] M. Čonková, V. Montes-García, M. Konopka, A. Ciesielski, P. Samori, A. R. Stefankiewicz, *Chem. Commun.* **2022**, *58*, 5773–5776.
- [83] Y.-H. Kang, X.-D. Liu, N. Yan, Y. Jiang, X.-Q. Liu, L.-B. Sun, J.-R. Li, *J. Am. Chem. Soc.* **2016**, *138*, 6099–6102.
- [84] L. X. He, C. R. Tian, J. H. Zhang, W. Xu, B. Peng, S. M. Xie, M. Zi, L. M. Yuan, *Electrophoresis* **2020**, *41*, 104–111.
- [85] S.-M. Xie, N. Fu, L. Li, B.-Y. Yuan, J.-H. Zhang, Y.-X. Li, L.-M. Yuan, *Anal. Chem.* **2018**, *90*, 9182–9188.
- [86] Z. Li, Z. Mao, W. Zhou, Z. Chen, *Anal. Chim. Acta* **2020**, *1094*, 160–167.
- [87] C. Wang, J. Shang, Y. Lan, T. Tian, H. Wang, X. Chen, J. Y. Gu, J. Z. Liu, L. J. Wan, W. Zhu, *Adv. Funct. Mater.* **2015**, *25*, 6009–6017.
- [88] M. Frank, S. Funke, H. Wackerbarth, G. H. Clever, *Phys. Chem. Chem. Phys.* **2014**, *16*, 21930–21935.
- [89] H. Wang, K. Wang, Y. Xu, W. Wang, S. Chen, M. Hart, L. Wojtas, L.-P. Zhou, L. Gan, X. Yan, Y. Li, J. Lee, X.-S. Ke, X.-Q. Wang, C.-W. Zhang, S. Zhou, T. Zhai, H.-B. Yang, M. Wang, J. He, Q.-F. Sun, B. Xu, Y. Jiao, P. J. Stang, J. L. Sessler, X. Li, *J. Am. Chem. Soc.* **2021**, *143*, 5826–5835.
- [90] J. L. Bolliger, T. K. Ronson, M. Ogawa, J. R. Nitschke, *J. Am. Chem. Soc.* **2014**, *136*, 14545–14553.
- [91] P. Mal, D. Schultz, K. Beyeh, K. Rissanen, J. R. Nitschke, *Angew. Chem. Int. Ed.* **2008**, *47*, 8297–8301.
- [92] H. P. Ryan, C. J. E. Haynes, A. Smith, A. B. Grommet, J. R. Nitschke, *Adv. Mater.* **2021**, *33*, 2004192.
- [93] S. Jiang, H. J. Cox, E. I. Papaioannou, C. Tang, H. Liu, B. J. Murdoch, E. K. Gibson, I. S. Metcalfe, J. S. O. Evans, S. K. Beaumont, *Nanoscale* **2019**, *11*, 14929–14936.
- [94] N. Sun, C. Wang, H. Wang, L. Yang, P. Jin, W. Zhang, J. Jiang, *Angew. Chem. Int. Ed.* **2019**, *58*, 18011–18016.
- [95] X. Hang, S. Wang, H. Pang, Q. Xu, *Chem. Sci.* **2022**, *13*, 461–468.
- [96] G. Melaugh, N. Giri, C. E. Davidson, S. L. James, M. G. Del Pópolo, *Phys. Chem. Chem. Phys.* **2014**, *16*, 9422–9431.
- [97] J.-H. Zhang, M.-J. Wei, Y.-L. Lu, Z.-W. Wei, H.-P. Wang, M. Pan, *ACS Appl. Energ. Mater.* **2020**, *3*, 12108–12114.
- [98] H. Mahdavi, S. J. D. Smith, X. Mulet, M. R. Hill, *Mater. Horiz.* **2022**, *9*, 1577–1601.
- [99] R. L. Greenaway, D. Holden, E. G. B. Eden, A. Stephenson, C. W. Yong, M. J. Bennison, T. Hasell, M. E. Briggs, S. L. James, A. I. Cooper, *Chem. Sci.* **2017**, *8*, 2640–2651.
- [100] N. O'Reilly, N. Giri, S. L. James, *Chem. Eur. J.* **2007**, *13*, 3020–3025.
- [101] P. Li, J. A. Schott, J. Zhang, S. M. Mahurin, Y. Sheng, Z.-A. Qiao, X. Hu, G. Cui, D. Yao, S. Brown, Y. Zheng, S. Dai, *Angew. Chem. Int. Ed.* **2017**, *56*, 14958–14962.
- [102] J. Zhang, S. H. Chai, Z. A. Qiao, S. M. Mahurin, J. Chen, Y. Fang, S. Wan, K. Nelson, P. Zhang, S. Dai, *Angew. Chem.* **2015**, *127*, 946–950.
- [103] T. D. Bennett, S. Horike, *Nat. Rev. Mater.* **2018**, *3*, 431–440.
- [104] R. Gaillac, P. Pullumbi, K. A. Beyer, K. W. Chapman, D. A. Keen, T. D. Bennett, F.-X. Coudert, *Nat. Mater.* **2017**, *16*, 1149–1154.
- [105] M. Costa Gomes, L. Pison, C. Červinka, A. Padua, *Angew. Chem. Int. Ed.* **2018**, *57*, 11909–11912.
- [106] N. Giri, M. G. Del Pópolo, G. Melaugh, R. L. Greenaway, K. Rätzke, T. Koschine, L. Pison, M. F. C. Gomes, A. I. Cooper, S. L. James, *Nature* **2015**, *527*, 216–220.
- [107] W. Shan, P. F. Fulvio, L. Kong, J. A. Schott, C.-L. Do-Thanh, T. Tian, X. Hu, S. M. Mahurin, H. Xing, S. Dai, *ACS Appl. Mater. Interfaces* **2018**, *10*, 32–36.
- [108] L. Ma, C. J. E. Haynes, A. B. Grommet, A. Walczak, C. C. Parkins, C. M. Doherty, L. Longley, A. Tron, A. R. Stefankiewicz, T. D. Bennett, J. R. Nitschke, *Nat. Chem.* **2020**, *12*, 270–275.
- [109] B.-N. T. Nguyen, J. D. Thoburn, A. B. Grommet, D. J. Howe, T. K. Ronson, H. P. Ryan, J. L. Bolliger, J. R. Nitschke, *J. Am. Chem. Soc.* **2021**, *143*, 12175–12180.
- [110] S. Ganta, C. Drechsler, Y.-T. Chen, G. H. Clever, *Chem. Eur. J.* **2022**, *28*, e202104228.
- [111] S. Saha, Y.-T. Chen, S. Ganta, M. Gilles, B. Holzapfel, P. Lill, H. Rehage, C. Gatsogiannis, G. H. Clever, *Chem. Eur. J.* **2022**, *28*, e202103406.
- [112] E. Garnett, L. Mai, P. Yang, *Chem. Rev.* **2019**, *119*, 8955–8957.
- [113] V. J. Babu, S. Vempati, T. Uyar, S. Ramakrishna, *Phys. Chem. Chem. Phys.* **2015**, *17*, 2960–2986.
- [114] A. Machín, K. Fontánez, J. C. Arango, D. Ortiz, J. De León, S. Pinilla, V. Nicolosi, F. I. Petrescu, C. Morant, F. Márquez, *Materials* **2021**, *14*, 2609.
- [115] N. Linares, A. M. Silvestre-Albero, E. Serrano, J. Silvestre-Albero, J. García-Martínez, *Chem. Soc. Rev.* **2014**, *43*, 7681–7717.
- [116] J. Dechnik, J. Gascon, C. J. Doonan, C. Janiak, C. J. Sumby, *Angew. Chem. Int. Ed.* **2017**, *56*, 9292–9310.
- [117] X. Liu, X. Wang, A. V. Bavykina, L. Chu, M. Shan, A. Sabetghadam, H. Miro, F. Kapteijn, J. Gascon, *ACS Appl. Mater. Interfaces* **2018**, *10*, 21381–21389.
- [118] E. V. Perez, K. J. Balkus, J. P. Ferraris, I. H. Musselman, *J. Membr. Sci.* **2014**, *463*, 82–93.
- [119] M. Jung, H. Kim, K. Baek, K. Kim, *Angew. Chem. Int. Ed.* **2008**, *47*, 5755–5757.
- [120] C. R. P. Fulong, J. Liu, V. J. Pastore, H. Lin, T. R. Cook, *Dalton Trans.* **2018**, *47*, 7905–7915.
- [121] Y. N. Yun, M. Sohail, J.-H. Moon, T. W. Kim, K. M. Park, D. H. Chun, Y. C. Park, C.-H. Cho, H. Kim, *Chem. Asian J.* **2018**, *13*, 631–635.
- [122] J. Ma, Y. Ying, Q. Yang, Y. Ban, H. Huang, X. Guo, Y. Xiao, D. Liu, Y. Li, W. Yang, *Chem. Commun.* **2015**, *51*, 4249–4251.
- [123] C. Zhao, N. Wang, L. Wang, H. Huang, R. Zhang, F. Yang, Y. Xie, S. Ji, J.-R. Li, *Chem. Commun.* **2014**, *50*, 13921–13923.
- [124] C. Zhao, N. Wang, L. Wang, S. Sheng, H. Fan, F. Yang, S. Ji, J. R. Li, J. Yu, *AIChE J.* **2016**, *62*, 3706–3716.
- [125] M. A. Andrés, A. Carné-Sánchez, J. Sánchez-Laínez, O. Roubeau, J. Coronas, D. Maspoch, I. Gascón, *Chem. Eur. J.* **2020**, *26*, 143–147.
- [126] M. Kitchin, J. Teo, K. Konstas, C. H. Lau, C. J. Sumby, A. W. Thornton, C. J. Doonan, M. R. Hill, *J. Mater. Chem. A* **2015**, *3*, 15241–15247.
- [127] A. F. Bushell, P. M. Budd, M. P. Atfield, J. T. A. Jones, T. Hasell, A. I. Cooper, P. Bernardo, F. Bazzarelli, G. Clarizia, J. C. Jansen, *Angew. Chem. Int. Ed.* **2013**, *52*, 1253–1256.
- [128] M. Lippi, M. Cametti, *Coord. Chem. Rev.* **2021**, *430*, 213661.

- [129] R. Küng, A. Germann, M. Krüsmann, L. P. Niggemann, J. Meisner, M. Karg, R. Göstl, B. M. Schmidt, *Chem. Eur. J.* **2023**, *29*, e202300079.
- [130] V. J. Pastore, T. R. Cook, *Chem. Mater.* **2020**, *32*, 3680–3700.
- [131] Z. Yang, G. Liu, Y. Di Yuan, S. B. Peh, Y. Ying, W. Fan, X. Yu, H. Yang, Z. Wu, D. Zhao, *J. Membr. Sci.* **2021**, *636*, 119564.
- [132] X. Guo, S. Xu, Y. Sun, Z. Qiao, H. Huang, C. Zhong, *J. Membr. Sci.* **2021**, *632*, 119354.
- [133] J. Liu, W. Duan, J. Song, X. Guo, Z. Wang, X. Shi, J. Liang, J. Wang, P. Cheng, Y. Chen, M. J. Zaworotko, Z. Zhang, *J. Am. Chem. Soc.* **2019**, *141*, 12064–12070.
- [134] D. Nam, J. Huh, J. Lee, J. H. Kwak, H. Y. Jeong, K. Choi, W. Choe, *Chem. Sci.* **2017**, *8*, 7765–7771.
- [135] A. V. Zhukhovitskiy, J. Zhao, M. Zhong, E. G. Keeler, E. A. Alt, P. Teichen, R. G. Griffin, M. J. A. Hore, A. P. Willard, J. A. Johnson, *Macromolecules* **2016**, *49*, 6896–6902.
- [136] Y. Wang, M. Zhong, J. V. Park, A. V. Zhukhovitskiy, W. Shi, J. A. Johnson, *J. Am. Chem. Soc.* **2016**, *138*, 10708–10715.
- [137] Y. Sun, C. Chen, P. J. Stang, *Acc. Chem. Res.* **2019**, *52*, 802–817.
- [138] Y. Gu, E. A. Alt, H. Wang, X. Li, A. P. Willard, J. A. Johnson, *Nature* **2018**, *560*, 65–69.
- [139] M. Herder, B. M. Schmidt, L. Grubert, M. Pätzelt, J. Schwarz, S. Hecht, *J. Am. Chem. Soc.* **2015**, *137*, 2738–2747.
- [140] A. V. Zhukhovitskiy, M. Zhong, E. G. Keeler, V. K. Michaelis, J. E. Sun, M. J. Hore, D. J. Pochan, R. G. Griffin, A. P. Willard, J. A. Johnson, *Nat. Chem.* **2016**, *8*, 33–41.
- [141] Y. Wang, Y. Gu, E. G. Keeler, J. V. Park, R. G. Griffin, J. A. Johnson, *Angew. Chem. Int. Ed.* **2017**, *56*, 188–192.
- [142] J. Zhao, L. Cheng, K. Liu, Z. Zhang, W. Yu, X. Yan, *Chem. Commun.* **2020**, *56*, 8031–8034.
- [143] A. Carné-Sánchez, G. A. Craig, P. Larpent, T. Hirose, M. Higuchi, S. Kitagawa, K. Matsuda, K. Urayama, S. Furukawa, *Nat. Commun.* **2018**, *9*, 2506.
- [144] A. Legrand, G. A. Craig, M. Bonneau, S. Minami, K. Urayama, S. Furukawa, *Chem. Sci.* **2019**, *10*, 10833–10842.
- [145] A. Legrand, L.-H. Liu, P. Royla, T. Aoyama, G. A. Craig, A. Carné-Sánchez, K. Urayama, J. J. Weigand, C.-H. Lin, S. Furukawa, *J. Am. Chem. Soc.* **2021**, *143*, 3562–3570.
- [146] Z. Wang, C. Villa Santos, A. Legrand, F. Haase, Y. Hara, K. Kanamori, T. Aoyama, K. Urayama, C. M. Doherty, G. J. Smales, B. R. Pauw, Y. J. Colón, S. Furukawa, *Chem. Sci.* **2021**, *12*, 12556–12563.
- [147] A. Carné-Sánchez, G. A. Craig, P. Larpent, V. Guillerme, K. Urayama, D. Maspocho, S. Furukawa, *Angew. Chem. Int. Ed.* **2019**, *58*, 6347–6350.
- [148] Z. Wang, G. A. Craig, A. Legrand, F. Haase, S. Minami, K. Urayama, S. Furukawa, *Chem. Asian J.* **2021**, *16*, 1092–1100.
- [149] J. A. Foster, R. M. Parker, A. M. Belenguer, N. Kishi, S. Sutton, C. Abell, J. R. Nitschke, *J. Am. Chem. Soc.* **2015**, *137*, 9722–9729.
- [150] M. M. Smulders, S. Zarra, J. R. Nitschke, *J. Am. Chem. Soc.* **2013**, *135*, 7039–7046.
- [151] R. Kumar, C. Rao, *Dalton Trans.* **2017**, *46*, 7998–8003.
- [152] T. Hu, X. Mei, Y. Wang, X. Weng, R. Liang, M. Wei, *Sci. Bull.* **2019**, *64*, 1707–1727.
- [153] N. R. Glavin, R. Rao, V. Varshney, E. Bianco, A. Apte, A. Roy, E. Ringe, P. M. Ajayan, *Adv. Mater.* **2020**, *32*, 1904302.
- [154] W. Zhu, A. Noureddine, J. Y. Howe, J. Guo, C. J. Brinker, *Nano Lett.* **2019**, *19*, 1512–1519.
- [155] M. Busi, M. Laurenti, G. G. Condorelli, A. Motta, M. Favazza, I. L. Fragalà, M. Montalti, L. Prodi, E. Dalcanale, *Chem. Eur. J.* **2007**, *13*, 6891–6898.
- [156] J. J. Garcia-Lopez, S. Zapotoczny, P. Timmerman, F. C. van Veggel, G. J. Vancso, M. Crego-Calama, D. N. Reinhoudt, *Chem. Commun.* **2003**, 352–353.
- [157] S. A. Levi, P. Guatterri, F. C. van Veggel, G. J. Vancso, E. Dalcanale, D. N. Reinhoudt, *Angew. Chem. Int. Ed.* **2001**, *40*, 1892–1896.
- [158] E. Menozzi, R. Pinalli, E. A. Speets, B. J. Ravoo, E. Dalcanale, D. N. Reinhoudt, *Chem. Eur. J.* **2004**, *10*, 2199–2206.
- [159] A. Mulder, T. Auletta, A. Sartori, S. Del Ciotto, A. Casnati, R. Ungaro, J. Huskens, D. N. Reinhoudt, *J. Am. Chem. Soc.* **2004**, *126*, 6627–6636.
- [160] Q.-H. Yuan, L.-J. Wan, H. Jude, P. J. Stang, *J. Am. Chem. Soc.* **2005**, *127*, 16279–16286.
- [161] H. Zhao, Y. Lei, *Adv. Energy Mater.* **2020**, *10*, 2001460.
- [162] C. A. Grande, R. Blom, V. Middelkoop, D. Matras, A. Vamvakeros, S. D. M. Jacques, A. M. Beale, M. Di Michiel, K. Anne Andreassen, A. M. Bouzga, *Chem. Eng. J.* **2020**, *402*, 126166.
- [163] H. Yuan, J. Tao, N. Li, A. Karmakar, C. Tang, H. Cai, S. J. Pennycook, N. Singh, D. Zhao, *Angew. Chem. Int. Ed.* **2019**, *58*, 14089–14094.
- [164] C. Wang, B. An, W. Lin, *ACS Catal.* **2019**, *9*, 130–146.
- [165] A. Zimpel, N. Al Danaf, B. Steinborn, J. Kuhn, M. Höhn, T. Bauer, P. Hirschle, W. Schrimpf, H. Engelke, E. Wagner, M. Barz, D. C. Lamb, U. Lächelt, S. Wuttke, *ACS Nano* **2019**, *13*, 3884–3895.
- [166] M. del Rio, G. Turnes Palomino, C. Palomino Cabello, *ACS Appl. Mater. Interfaces* **2020**, *12*, 6419–6425.
- [167] L. Feng, H.-B. Hou, H. Zhou, *Dalton Trans.* **2020**, *49*, 17130–17139.
- [168] H. Deng, S. Grunder, K. E. Cordova, C. Valente, H. Furukawa, M. Hmadeh, F. Gándara, A. C. Whalley, Z. Liu, S. Asahina, H. Kazumori, M. O’Keeffe, O. Terasaki, J. F. Stoddart, O. M. Yaghi, *Science* **2012**, *336*, 1018–1023.
- [169] Y.-C. Luo, K.-L. Chu, J.-Y. Shi, D.-J. Wu, X.-D. Wang, M. Mayor, C.-Y. Su, *J. Am. Chem. Soc.* **2019**, *141*, 13057–13065.
- [170] S. Chen, K. Li, F. Zhao, L. Zhang, M. Pan, Y.-Z. Fan, J. Guo, J. Shi, C.-Y. Su, *Nat. Commun.* **2016**, *7*, 13169.
- [171] K. Li, L.-Y. Zhang, C. Yan, S.-C. Wei, M. Pan, L. Zhang, C.-Y. Su, *J. Am. Chem. Soc.* **2014**, *136*, 4456–4459.
- [172] A. A. Talin, A. Centrone, A. C. Ford, M. E. Foster, V. Stavila, P. Haney, R. A. Kinney, V. Szalai, F. El Gabaly, H. P. Yoon, F. Léonard, M. D. Allendorf, *Science* **2014**, *343*, 66–69.
- [173] L. Sun, M. G. Campbell, M. Dincă, *Angew. Chem. Int. Ed.* **2016**, *55*, 3566–3579.
- [174] J. Lee, D.-W. Lim, S. Dekura, H. Kitagawa, W. Choe, *ACS Appl. Mater. Interfaces* **2019**, *11*, 12639–12646.
- [175] B. C. Wang, Z. Y. Feng, B. B. Hao, C. X. Zhang, Q. L. Wang, *Chem. Eur. J.* **2021**, *27*, 12137–12143.
- [176] X. Qiu, W. Zhong, C. Bai, Y. Li, *J. Am. Chem. Soc.* **2016**, *138*, 1138–1141.

Manuscript received: May 29, 2023

Accepted manuscript online: July 14, 2023

Version of record online: ■■■, ■■■

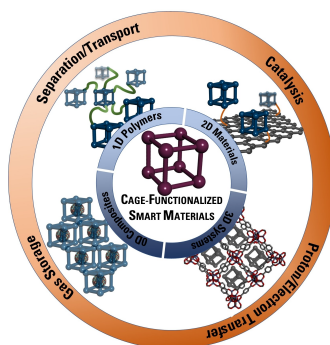
## Reviews

### Metal-Organic Cages

W. Drożdż, A. Ciesielski,\*

A. R. Stefankiewicz\* — e202307552

Dynamic Cages—Towards Nanostructured Smart Materials



Given their chemical and structural variability, dynamic organic and coordination cage architectures are increasingly being used in the formation of more complex systems—smart materials. In this Review we present basic know-how for modifying active surfaces with cage systems. The structure-dependent relationship between the cage used and the potential application of the obtained systems are also discussed.